Journal of Molecular Liquids 398 (2024) 124240

Contents lists available at ScienceDirect

Journal of Molecular Liquids

journal homepage: www.elsevier.com/locate/molliq

Role of surface functionalization and biomolecule structure on protein corona adsorption and conformation onto anisotropic metallic nanoparticles

Valeria Figueroa [a,b], Brenda Velasco [a], Lilia G. Arellano [a], Vicente Domínguez-Arca [a], Adriana Cambón [a], Alberto Pardo [a], Antonio Topete [a,b], Luis C. Rosales-Rivera [c], J.F. Armando Soltero [c], Silvia Barbosa [a,*], Pablo Taboada [a,*]

[a] Grupo de Física de Coloides y Polímeros, Departamento de Física de Partículas; Facultad de Física; Instituto de Materiales (IMATUS) e Instituto de Investigaciones Sanitarias (IDIS), Universidade de Santiago de Compostela, 15782-Santiago de Compostela, Spain
[b] Departamento de Fisiología, Centro Universitario de Ciencias de la Salud (CUCS), Universidad de Guadalajara, Guadalajara, 44340, Mexico
[c] Departamento de Ingeniería Química, CUCEI, Universidad de Guadalajara, Guadalajara. Mexico

ARTICLE INFO

Keywords:
Gold nanorod
Protein corona
Surface functionalization
Cooperative interactions

ABSTRACT

In the biological milieu, nanoparticles (NPs) interact with different biomolecules, particularly proteins, leading to the formation of an interfacial corona, which gives rise to a new biological identity affecting NP biodistribution, cytotoxicity and biological fate. The surface coating of NPs plays a key role in regulating such biocorona formation and composition. We here investigated the interactions between bovine serum albumin (BSA) and bovine fibrinogen (FIB) with gold nanorods (Au NRs) bearing different surface coatings (cetyltrimethylammonium bromide, CTAB, and carboxylic acid and amine-terminated polyethylene glycols (PEGs). It was revealed that CTAB-coated NPs interact with both proteins with high affinity (ca. 10^8-10^9 M^{-1}) whereas for PEG ones the extent of protein binding decreases thanks to the stealth properties of PEG, but a protein corona is still formed, with binding affinities between 10^4-10^6 M^{-1}. In addition, present results indicated that thicknesses of protein coronas and the aggregation behavior of AuNPs were closely related to their surface properties and protein structure. We also found that BSA and FIB underwent different conformational changes upon adsorption depending on the surface-modified Au NRs. Hence, these findings offered important insights into the essence of the interactions between NPs and proteins toward the development of safe and effective nanomaterials.

1. Introduction

The advent of nanotechnology into medicine is being translated during last decades in huge efforts by researchers of different fields of science and clinicians to configure truly personalized health care (also known as *precision medicine*) by developing novel strategies, contrast agents and imaging techniques, and biological and drug compounds to look for the full, successful recovery of diseases such as cancers, infections, cardiovascular and neuropathologies whilst avoiding undesired side toxic effects [1]. A particular focus in this regard has been paid to control and regulate the systemic administration of chemical and biological-based drugs and compounds, looking for maximization of the therapeutic responses at optimized, minimal administered doses in the specific site of action while hindering their degradation and fast excretion from human body [2].

To achieve such goals, one widely used approach has been the encapsulation of the bioactive compound(s) inside the so-called nanocarriers, structural entities of organic (lipidic, polymeric, carbon-based ones), inorganic (metallic, ceramic, oxide…) or biological (protein, virus, cell) nature and with sizes generally below one micron, which offer i) protection for the encapsulated cargo to the hostile physiological environment; ii) an enhancement of the solubilization capacity; iii) the transport and delivery of the loaded molecules to the site of action and their subsequent selective accumulation in the diseased areas through, for example, the enhanced permeation and retention (EPR) effect [3]; iv) the evasion from opsonization and macrophage recognition, then, achieving extended circulation times. In addition, these nanocarriers can be further modified to incorporate additional moieties or functional

* Corresponding authors.
E-mail addresses: silvia.barbosa@usc.es (S. Barbosa), pablo.taboada@usc.es (P. Taboada).

https://doi.org/10.1016/j.molliq.2024.124240
Received 22 November 2023; Received in revised form 5 February 2024; Accepted 7 February 2024
Available online 10 February 2024

groups able to bind overexpressed or transformed molecular targets in the diseased cells or tissues [4,5] thus, favoring the selective homing to the desired site of action.

Among the different types of nanocarriers, those based on gold nanoparticles (Au NPs) are particularly appealing thanks not only to their capacity to transport drugs by adsorption or conjugation [6,7], but also by their special optical (plasmonic) properties -which can be modified by simply changing their morphology and size, their colloidal stability, nontoxicity, nonreactivity, and ease for surface functionalization through well-established (bio)chemical methods, among other advantages [8]. In particular, Au NPs with anisotropic, rod-like structure known as gold nanorods (Au NRs) have the ability to absorb (but also scatter) light both in the visible and near-infrared (NIR) region of the electromagnetic spectrum with relatively high efficiency thanks to the development of both transverse (TSPR) and longitudinal localized surface plasmon resonances (LPSR), respectively, which can allow their exploitation in different biomedical applications including bioimaging, diagnosis, therapy and biosensing, amongst others[9,10], even reaching clinical trials [4,11]. The anisotropic structure of Au NRs may favor i) the transformation absorbed light within the first biological window (NIR electromagnetic spectrum) into localized heat with high efficiency as a consequence of their large absorption cross section [12], allowing their potential use as thermal nanoagents for photothermal treatment, ii) as well as their internalization within different types of cells [6,11].

Nevertheless, to carry out their intended transport, delivery, imaging and/or therapeutic functions, it is crucial to understand the fate of Au NRs upon administration in the human body and, if possible, to attempt its control. Among the different parameters which can dictate the Au NR colloidal stability, biodistribution, residence time, and uptake within cells and tissues once administered *in vivo*, NP surface chemistry plays a key role since it regulates the interactions between Au NRs and the proteins and other biomolecules present in the biological milieu and which can potentially absorb onto the particle surface, forming the so-called protein corona [13]. This is recognized as the main element in modulating NP toxicity, biodistribution, metabolism, cellular internalization in biological systems [14,15]. In other words, the biological identity of metallic NPs and Au NRs, that is, "what cells see", will be the inorganic core plus the surrounding coating layer of adsorbed proteins. This bioidentity may differ depending on the composition of the protein coating layer [16,17], which will be largely affected by the NP synthetic identity, that is, its structure, composition, morphology, nature of surface coating and charge, etc, and the surrounding biological environment. Numerous systematic works have been conducted to elucidate the influence of one or more of these parameters in the mechanism and kinetics of protein corona formation, the elucidation of its composition and dynamic evolution for spherical NPs [18,19]; however, and despite their wider range of theranostic applications, these studies are relatively scarcer for anisotropic ones as Au NRs [20,21].

Previous reports have addressed the issue of correlating AuNR physicochemical properties with the interplay of model NP libraries with cells and proteins, in which factors such as particle size [22], particle charge [16], temperature [17], hydrophobicity [23], particle surface groups [24], and so forth, were systematically varied. Several works have focused on the interactions between different proteins and Au NRs with different surface modifications (peptides, polymers, surfactants with amine, carboxyl, hydroxyl and other bearing functional groups) since surface chemistry plays a critical role in the NP's fate and biological behavior [25,26]. Strategies based on polymer grafting onto the NPs have been widely used for tailoring NP surface characteristics such as offering different functionalities for bioconjugation of homing ligands and improving NR colloidal stability in media of biological relevance [18]. Poly(ethylene glycol) (PEG) is commonly used to provide NPs with colloidal stability by means of electrostatic and steric interactions as well as to reduce protein unspecific adsorption [27]. However, PEG layer(s) cannot completely hinder protein adsorption onto the NP metallic surface [2,7,23]. In addition, surface charge is also significant for defining the formation of protein corona and its composition, while having a clear subsequent impact on particle biodistribution [23,28]. For instance, positively charge Au NPs are rapidly identified by opsonins and cleared by the reticuloendothelial system (RES) or mononuclear phagocytic system (MPS), causing their rapid depletion in the body, and carboxylated PEG molecules, when deprotonated, are a highly effective in increasing the biocompatibility and blood circulation time of drug delivery nanocarriers. Moreover, protein structure and affinity by (nano)surfaces are also key in defining the composition and kinetics of the protein corona and the conformational stability of Au NR-bound proteins [29,30]. Thus, there is still plenty of work remaining in order to completely elucidate the influence of surface chemistry properties on the underlying specific interactions and kinetics between anisotropic NPs as Au NRs and physiological proteins toward the development of safe and effective bionanomaterials.

On the basis of the considerations made above, herein, we synthesized Au NRs of dimensions 39 × 9.5 nm and LPSR centered at ca. 798 nm which were surface-modified with cetyltrimethylammonium bromide, CTAB, and two heterobifunctional PEGs of 5 kDa bearing one thiol group on one side to facilitate the conjugation of the polymer onto the NP surface by Au-S bonding, and different terminal moieties: amine and carboxyl on the other side of the polymeric backbone to render the NP with positive or negative electric surface charge under suitable conditions, respectively. We selected bovine serum albumin, BSA, and bovine fibrinogen, FIB, as model proteins since they are the most abundant in blood plasma but very different in size, morphology and binding affinity to hydrophilic and hydrophobic surfaces; moreover, serum albumin and fibrinogen are amongst the most abundant proteins identified in the Au NP-biocorona after exposure to fresh human blood plasma and serum [30]. Following a bottom-up approach (one type of protein interacting with one type of NP), we have investigate the interactions of both proteins with the different surface-coated Au NRs to decipher the role played by surface chemistries, surface charges and protein structure/morphology in the nature of t their concomitant interactions as well as the dynamics of protein-Au NR binding, and the potential induced conformational changes of the adsorbed protein molecules, which may significantly impact the biological identity of the nanomaterial, as mentioned previously.

2. Experimental section

2.1. Materials

Hexadecyltrimethyl ammonium bromide for molecular biology (CTAB), tetrachloroauric acid ($HAuCl_4 \cdot 3H_2O$ > 99.9 %), silver nitrate ($AgNO_3$), sodium borohydride ($NaBH_4$), bovine serum albumin (BSA), bovine fibrinogen (FIB) and phosphate buffer saline (PBS) were purchased from Sigma-Aldrich. Heterobifunctional PEG polymers were from Laysan Bio Inc (Arab, AL, USA). Ascorbic acid was from Fluka, whereas Bradford assay was from Invitrogen (Carlsbad, CA, USA) All other reagents were of analytical grade. All chemicals were used as received. Milli-Q water (Millipore) was used throughout all the experiments.

2.2. Synthesis of Au NRs

Au NRs were synthesized using a modified seed-mediated growth method [31]. First, CTAB-capped Au seeds were obtained. To do that, 7.5 mL of a 0.2 M CTAB solution was gently mixed with 0.25 mL of 0.01 M $HAuCl_4$ in a water bath at 28 °C. As an indication, for both seeds and Au NRs preparation, CTAB was left at a constant temperature of 28 °C for one day under constant stirring of 100 rpm to achieve full solubilization and avoid foaming prior to use. Next, a 0.01 M $NaBH_4$ solution was prepared in ice-cold water. This solution was left to rest for 2–3 min to ensure a good dispersion of the reductant. Afterwards, while the Au-CTAB solution was stirred at 200 rpm, 0.6 mL of ice-cold 0.01 M $NaBH_4$

were added in one pull to the former, after which the mixed solution turned brownish yellow. This solution was mixed gently by hand for 2 min and then left un-disturbed in a water bath at 28 °C for 1 h to allow the excess sodium borohydride to be decomposed.

For the growth of Au NRs, 4.25 mL of a 0.01 M $HAuCl_4$ solution were added to 100 mL of 0.2 M CTAB in a water bath at 28 °C, after which the solution turned bright yellow while stirred at 500 rpm. Then, 1.23 mL of a 0.01 M of an $AgNO_3$ solution (prepared in darkness) was added to the Au growth solution followed by gentle mixing at 500 rpm. Then, 680 μL of a 0.1 M ascorbic acid (AA) solution were added followed by gentle stirring at 500 rpm until the solution turned colourless (ca. 4 min). Finally, 1.1 mL of the Au seed solution were gently added to the Au growth solution while stirring for 2 min and then stopped. The resulting solution was left undisturbed in a water bath overnight at 28 °C for ca. 12 h becoming reddish-pink. The formed Au NRs were centrifuged at least twice at 28 °C for 30 min at ca. 20000g and redispersed in 10 mL of deionized water. The concentration of Au NRs was determined spectrophotometrically and by inductively coupled plasma mass spectrometry (ICP-MS), when needed.

2.3. Pegylation of Au NRs

The synthesized Au NRs were modified with different PEGs to study the effect of the Au NR surface charge on the interaction with BSA and FIB. Two different surface charge Au NR samples were prepared using two PEG polymers (sharing virtually an equal molecular weight of 5 kDa): negatively charged (HS-PEG-COOH) and positively charged (HS-PEG-NH_2) PEGs (see Fig. 1a). In general, an excess of 18,000 PEG chains per Au NR (~16 PEG/nm^2 of Au NR) were added to ensure the total coverage of the Au NR surface [32]. The PEG addition was done in two steps as reported in a previous work to ensure complete Au NR detoxification (CTAB removal) [21]. Briefly, in the first step, a calculated amount of PEG was added to a final concentration of 10 nM Au NRs and the solution was stirred at 350 rpm overnight. The suspension was centrifuged for 30 min at 14500 rpm at 25 °C and resuspended in 1 mL of water. In the second step, the same amount of PEG was added to 5 mL of methanol 90 % and then the pellet from centrifugation (Au NRs) was added to this solution and stirred for 5 h at 350 rpm. Next, the solution was centrifuged for 30 min at 14500 rpm at 25 °C, resuspended in deionized water and stored at 4 °C for further characterization.

To determine the PEGylation coverage of Au NRs, potentiometric titration measurements were made. Briefly, 0.5 mL of NaOH 15 mM were added to a 2.5 mL solution PEGylated Au NRs (either 5.8 nM PEG-COOH- or 6.7 nM PEG-NH_2-coated ones, respectively) initially at pH 5.0 to reach a final pH of 11.5. Next, titrations from 2 to 25 μL of a HCl solution (25 or 50 mM) into the former solution were made in 2 min-intervals under stirring, the solution was stirred for 1 min, and the pH measured. The (de)protonation of PEG chains could be calculated from the following equations:

$$V_A = \sum_{i=0} Vt_i$$

$$H_c^+ = \sum_{i=0} Vt_i \times 10^{-6} \times [H_t^+]_i \quad (1)$$

$$[H^+]_c = \frac{H_c^+}{V_0 + V_A \times 10^{-3}}$$

where i is the titration number; V_A the accumulated volume; V_t the titration volume; H_c^+ the H^+ amount accumulated in solution (μmol); $[H_t^+]_i$ the H^+ concentration in each titration; and $[H^+]_c$ the H^+ concentration accumulated in solution. The extent of PEGylation was derived from the first derivative of the plot pH *vs.* H^+ using the equation:

$$PEG : NP = \frac{(2Å^o inflection - 1Å^o inflection)}{[NP]_0 \times V_0} \quad (2)$$

where *PEG:NP* is the number of PEG chains per NP; V_0 the initial volume of the NP solution; and $[NPs]_0$ the initial Au NRs concentration.

2.4. Preparation of the bioconjugates

Prior to use, BSA and FIB were purified by size exclusion liquid chromatography using a Superdex 75 column equilibrated with 0.01 M phosphate buffer (PBS). Protein-coated AuNRs were prepared by adding a suitable volume of the protein stock solution (1 mg/mL for BSA and 2 mg/mL for FIB, respectively) to 1.3 mL of an AuNR solution (2 nM), and the final volume adjusted to 1.75 mL. The bioconjugate solution was

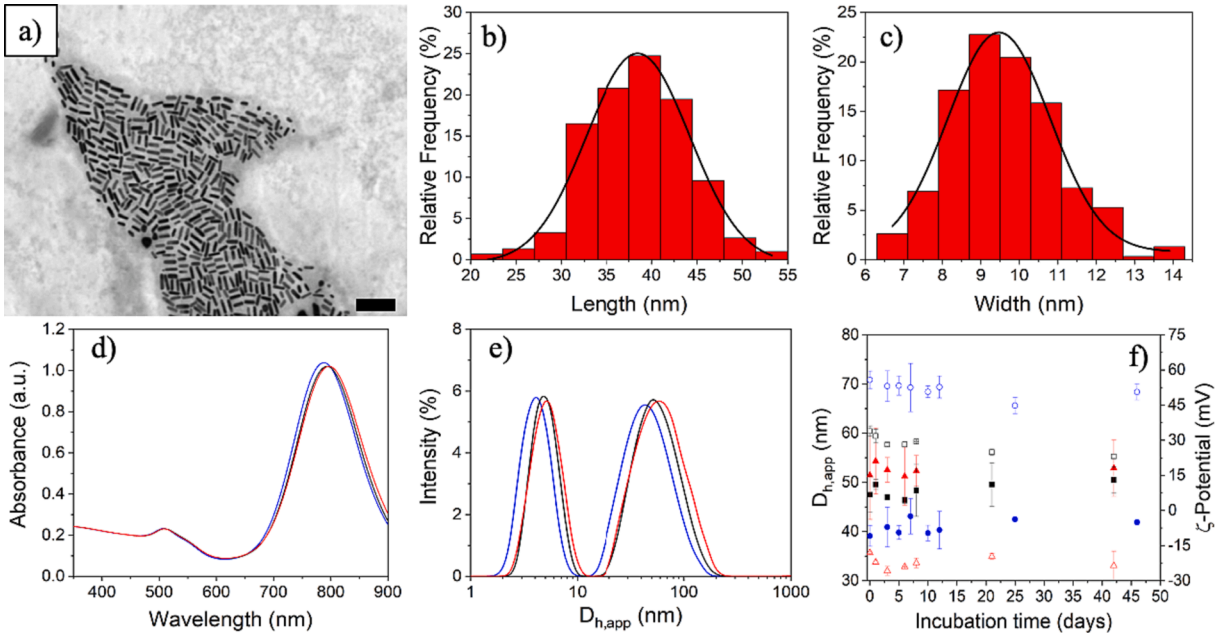

Fig. 1. a) STEM image of CTAB-coated Au NRs. Population b) length and c) width distributions of the as-synthesized CTAB-coated Au NRs. d) UV–Vis spectra; e) population size distribution obtained by DLS of CTAB- (——), PEG-COOH- (—) and PEG-NH_2- (——) coated Au NRs; f) temporal evolution of hydrodynamic sizes and surface potential of (●,○) CTAB-, (■,□)PEG-COOH-, and (▲,△) PEG-NH_2-coated AuNRs.

stirred at 300 rpm at 25 °C for 2 h. Next, the protein bioconjugates were centrifuged at 13000g for 30 min at 25 °C and collected by redispersion in 450 μL of water. Different theoretical NP surface saturation ratios, the number of times exceeding the required protein concentration to achieve the theoretical saturation of the NP surface, between 0 and 10 were analyzed (that is, protein:NP molar ratios between 0 and 1000 and 0 to 200 for BSA and FIB, respectively). For such purpose, the formation of the protein corona monolayer was obtained as the ratio of the Au NR surface area regarding the effective cross-sectional area of the protein; to this end, the geometry of BSA was considered as a sphere, whereas that of FIB as a cylinder. The protein concentration was determined spectrophotometrically using a molar absorption coefficient of 43,824 and 513400 M^{-1} cm^{-1} at 280 nm for BSA and FIB, respectively [2,33].

On the other hand, fluorescently labeled BSA and FIB (BSA@FITC and FIB@FITC) were used as model proteins to follow the protein corona formation and determine the extent of protein adsorption onto the NPs. Both proteins were labeled with fluorescein isothiocyanate (FITC) at a molar ratio FITC: protein of 8 following previous reports [15]. Very briefly, 300 μL of a 5 mg/mL FITC solution in DMSO were added very slowly to a 10 mg/mL BSA carbonate buffer solution (0.1 M, pH 9). The reaction was maintained for 4 h at 25 °C in dark. After incubation the protein solution was centrifuged at 14500 rpm and re-suspended in fresh PBS buffer to remove the unbound protein. Next, remaining free dye was cleared out using a Sephadex G-25 column equilibrated with 25 mL PBS. The final protein concentration and labeling extent were confirmed by UV–Vis and fluorescence spectroscopies.

The amount of the adsorbed protein molecules onto the different types of Au NRs was obtained by analyzing the amount of fluorescently-labeled protein in the supernatants after conjugation by means of fluorescence spectroscopy in the wavelength range of from 300 to 750 nm upon excitation at 495 nm, using 5 nm/5 nm slit widths in a Cary Eclipse spectrofluorometer (Varian Instruments Inc.). Each spectrum was the average of three scans. Values were compared with those from a previous obtained for a developed calibration curve. The amount of protein adsorbed onto the NPs was considered as the difference between the initially injected protein concentration and that measured in the supernatants. In addition, the protein concentration in the supernatants was also measured by means of the Bradford assay following the manufactureŕs instructions for comparison.

2.5. Physico-chemical characterization of protein-Au NR interactions and Au NRs-based bioconjugates

2.5.1. UV–Vis absorbance spectroscopy

UV–vis spectroscopy was performed in the absence and presence of proteins with a Cary Bio 100 UV–vis spectrophotometer (Agilent Technologies, USA) using 1 cm quartz cells. For measurements, pure Au NRs in the absence and presence of different protein concentrations (300 μL) were placed in a cuvette and spectral analysis was performed in the 350–900 nm range. BSA and FIB concentrations added to the Au NR solution (2 nM) were changed between 0 and 2 μM for BSA, and 0 and 0.4 μM for FIB, respectively, and the same protocol described for the incubation and removal of free protein was followed. Each sample solution was measured three times to ensure reproducibility and averaged to produce a single spectrum.

2.5.2. Fluorescence spectroscopy

Intrinsic tryptophan, tyrosine and phenylalanine fluorescence quenching induced by Au NRs was recorded with a Cary Eclipse fluorescence spectrophotometer equipped with a temperature controller and a multicell sample holder (Varian Instruments Inc.). The fluorescence emission spectra were measured at 25 °C in PBS (0.01 M, pH 7.4) in solutions of Au NRs (600 μL) placed in a quartz cuvette at different NP concentrations (0–0.75 nM) and recorded in the wavelength range from 300 to 400 nm upon excitation at 280 nm. Each spectrum was the average of three scans. Rather similar protein (3 and 0.23 μM for BSA and FIB, respectively) and particle concentrations as in UV–Vis absorbance measurements were measured.

2.5.3. Dynamic light scattering (DLS) and zeta potential measurements

Hydrodynamic Au NR diameters in the absence and presence of protein molecules were measured using a Zetasizer Nano ZS (Malvern, Instruments, UK). For size distribution measurements, the samples were diluted with MilliQ water in cuvettes with a 1 cm optical path. The bioconjugates were incubated for 30 min, after which seven DLS measurements were taken, where the maximum size change was selected for comparison. Zeta potential measurements were acquired with the same instrument from 30 runs for each sample, where each value was the average of at least seven independent measurements.

2.5.4. Circular dichroism (CD) spectroscopy

CD spectra were acquired with a Jasco-715 automatic recording spectropolarimeter at room temperature with a JASCO PTC-343 Peltier-type thermostated cell holder (Jasco, Japan). Quartz cuvettes with 0.2 cm path length were used. The CD spectra were recorded from 190 to 250 nm, and the bandwidth was set to 1 nm. PBS (0.01 M, pH 7.0) alone, without protein, was used as a blank. BSA (2 μM) and FIB (0.4 μM) were measured in the absence and presence of Au NRs (0.5–5 nM) with different coatings. The final spectra were obtained by subtracting the buffer contribution from the original protein spectra, and all measurements were repeated in triplicate. The mean residue ellipticity θ (deg cm^2 $dmol^{-1}$) was calculated from the formula $\theta = (\theta_{obs}/10)(MRM/lc)$, where θ_{obs} is the observed ellipticity in deg, *MRM* is the mean residue molecular mass, *l* is the optical path-length (in cm), and *c* is the protein concentration (in g mL^{-1}). To calculate the composition of the secondary structure of the protein, SELCON3, CONTIN, and DSST programs were used to analyze far-UV CD spectra using the CDPro software. Final results were assumed when data generated from all programs show convergence.

2.5.5. Transmission electron microscopy (TEM)

All Au NRs were visualized prior to and following the formation of the protein corona by TEM (JEOL JEM 1011, Japan) at an accelerating voltage of 200 kV. The samples were diluted prior to TEM observation and subsequently, a drop from each colloid was placed onto a carbon-coated copper grid. Any excess suspension was removed using filter paper.

2.5.6. Fourier transform infrared spectroscopy (FTIR)

FTIR were recorded using an Agilent 670 FTIR instrument (Agilent, USA). All measurements were performed using the ATR method, with a resolution of 2 cm^{-1} in the range from 4500 to 500 cm^{-1}. Generally, 400 scans were accumulated to get a reasonable signal-to-noise ratio. Solvent spectra were also examined in the same accessory and instrument conditions. Each final sample spectrum was obtained by digitally subtracting that of the solvent from the corresponding raw sample spectrum. Each sample solution was measured three times to ensure reproducibility and averaged to produce a single spectrum. BSA (2.0 μM) and FIB (0.4 μM) were measured in the absence and presence of AuNPs in PBS (0.01 M, pH 7.4).

2.5.7. Isothermal titration calorimetry

The isothermal calorimetric measurements were performed in triplicate using a VP-ITC microcalorimeter (MicroCal, LLC.). BSA (0.17 and 36 μM) and FIB (0.034 and 7.2 μM) were titrated into 1.8 mL of Au NR solution in 0.25X PBS buffer pH 7.4 at ca. 2 nM inside the reaction cell. The first injection of 0.5 μL (which is removed from the analysis) was followed by 28 injections of 10 μL volume. During all the experiments the temperature of the ITC device was kept constant at 37 °C. The respective protein solutions were titrated into PBS buffer to establish the baseline analysis. A background correction was done to account for the heat of dilution by subtracting the data of titration of the corresponding

protein solution onto the PBS buffer. The experimental data were fitted to a one-site or two-sites (when corresponding) binding model by using the ORIGIN® software implemented in the instrument's software supplied by MicroCal.

3. Results and discussion

3.1. Synthesis and characterization of CTAB- and PEG-coated Au NRs

As-synthesized CTAB-coated Au NRs, were prepared by means of a well-established two-step seed-mediated growth method with slight modifications (see Experimental section for details) [31]. They exhibited a size of ca. 39 × 9.5 nm with an aspect ratio of 4.05 as observed by TEM (Fig. 1a-c), a surface charge of 56.3 ± 4.4 mV and two well-defined plasmon bands: a weak, shorter transversal plasmon one at ca. 508 nm and a stronger longitudinal one at ca. 798 nm, respectively (see Fig. 1d). The CTAB-Au NR size population distribution obtained by DLS revealed two different peaks which stem from the morphological anisotropy of Au NRs (Fig. 1e); the size distribution peak at smaller $D_{h,app}$ values corresponds to the rotational diffusion coefficient and the second to the translational diffusion coefficient [34]. It is here necessary to remind that the hydrodynamic size obtained from DLS is based on the assumption of a spherical morphology, however, the size distribution associated to the rotational diffusion does not represent an actual particle size, neither the transverse or longitudinal dimensions of the Au NRs, but means that their rotational diffusion coefficient is similar to the translational diffusion coefficient of a sphere with that diameter. DLS data showed that CTAB-coated Au NRs were very stable in aqueous solution for long periods of time (up to 50 days) in PBS buffer (137 mM NaCl, 2.7 mM KCl, 8 mM Na_2HPO_4, and 2 mM KH_2PO_4) enabling their

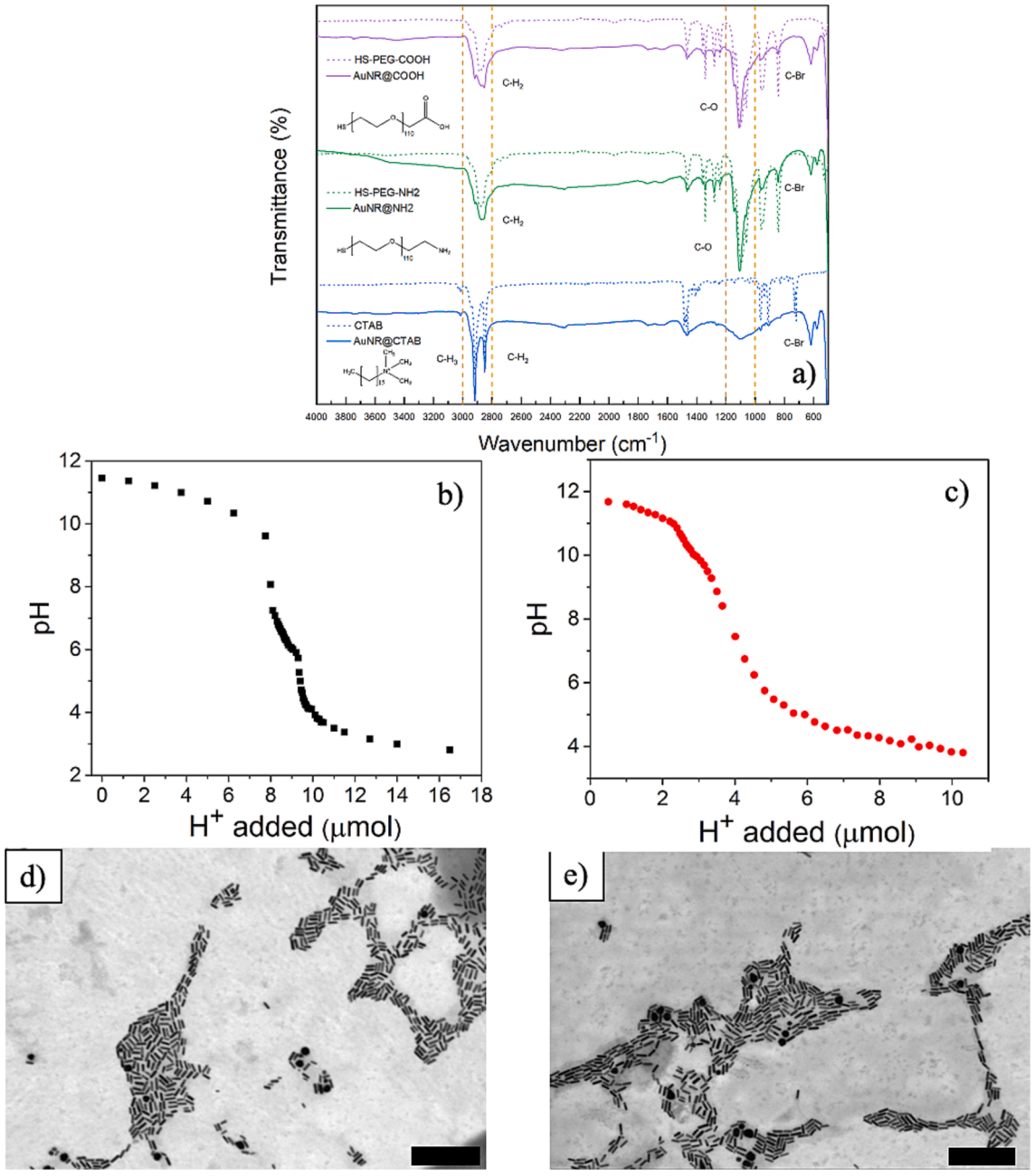

Fig. 2. a) FTIR spectra of CTAB- (——), PEG-COOH- (——), and PEG-NH_2- (——) coated Au NRs. Potentiometric titration of b) PEG-COOH- (■) and c) PEG-NH_2- (●) coated Au NRs. STEM images of d) PEG-COOH- and e) PEG-NH_2-coated Au NRs.

storage for further use, as confirmed by the temporal evolution of their hydrodynamic sizes and surface charges, which remain barely invariable (Fig. 1f).

To provide the metallic particles with colloidal stability and stealthiness in physiological-mimicking media as well as to eliminate most of toxic CTAB molecules adhered to the Au NR surfaces after the synthesis and subsequent washing steps and mask the potential remaining ones, Au NRś surfaces were functionalized with two different heterobifunctional PEG polymers of 5 kDa bearing carboxyl and amine end groups (PEG-COOH and PEG-NH_2, respectively) via a ligand exchange process by means of Au-thiol bonding. For such purpose, Au NRs volume and mass were calculated according to the dimensions of the metallic NPs obtained by TEM and their metal concentration by inductively coupled plasma mass spectrometry (ICP-MS). The successful PEGylation of Au NRs was corroborated by FTIR, UV–Vis spectra, potentiometric, surface charge, TEM and DLS measurements.

FTIR spectra (Fig. 2a) confirmed the presence of the characteristic bands of PEG corresponding to C–O symmetric stretching (ca. 1110 cm^{-1}), C–H stretching (ca. 1016 cm^{-1}) and aliphatic C–H bending (ca. 1407, 2926 and 2857 cm^{-1}) vibrations [35]. Potentiometric titrations of PEG-NH_2 and PEG-COOH-coated Au NRs additionally confirmed the successful coating of the metal NPs with both types of PEG polymers as confirmed by the changes in the protonation state of the metallic NPs upon HCl titration, which allowed to estimate the amount of PEG chains on Au NRs surfaces. In particular, Fig. 2b shows the presence of two clear equivalent points for PEG-COOH-coated AuNRs. The first one corresponds to the initial and progressive protonation of COOH groups on the extended weak polyacid, whereas the second one might be related to an additional moiety protonation due to a potential conformational transition from an extended configuration of PEG to a more coiled state, a well-known phenomenon for weak polyelectrolytes and relatively low molecular weight weak acids [36]. Similar equivalence points were found for PEG-NH_2-coated Au NRs, but with a much smoother profile (Fig. 2c). Considering the concentration of Au NRs used (5.8 and 6.7 nM for PEG-COOH and PEG-NH_2-coated Au NRs, respectively), averaged numbers of PEG-COOH and PEG-NH_2 chains onto the Au NR were estimated to be 98 ± 11 and 77 ± 9, respectively. Since the mean surface area of an Au NR is ca. 1350 nm^2, a coverage density of 0.073 and 0.057 for COOH and NH_2 groups per nm^2 was determined, in agreement with previous reports [22]. The presence of a compact bilayer of CTAB on the surface of Au NRs may be responsible for the low coverage density of PEG chains on the surface of CTAB-capped metallic NPs after ligand exchange [37]. This behavior contrasts with the facile ligand substitution observed in citrate-capped Au NPs [38], and as evidenced in the following sections, the persistence of CTAB and the low coverage density with PEG had a strong influence on the protein-Au NRs interactions.

The PEG coating was also corroborated by the changes observed in ζ-potential values upon PEG functionalization, from ca. 56.3 ± 3.4 for CTAB-coated Au NRs to -17.5 ± 3.4 and 33.9 ± 3.4 for PEG-COOH and PEG-NH_2, respectively. The Au NRs did not suffer any change in size or morphology as observed by TEM (Fig. 2d-e) after PEGylation, with no signs of particle aggregation. The absence of significant longitudinal plasmon shifts or peak broadening also confirmed this point (Fig. 1d). At this respect, small increases were observed in NP hydrodynamic sizes after the ligand exchange process from ca. 39 ± 4 to ca. 51 ± 4 and 47 ± 6 nm for PEG-COOH- and PEG-NH_2-coated Au NRs, respectively, which stemmed from the larger size of the PEG chain than the CTAB molecules (Fig. 1e). Considering that a single PEG monomeric unit is 44 Da in weight and 0.35 nm in length, the contour lengths of the present PEG chains (i.e., the length of PEG in hypothetically fully stretched conformation), with M_w of 5 kDa would amount to, ca. 40 nm. Nonetheless, the observed enlargement in the hydrodynamic radius following PEGylation is merely within the range of 8 to 12 nm for the two distinct PEG chains. This clearly suggests that the PEG chains are not extended but rather arranged in a coiled, folded, or twisted manner on the surface of the NP. This finding aligns entirely with prior studies [7,39].

On the other hand, the conformation of PEG chains grafted on Au NRs can be estimated by applying the *Alexander – de Gennes* theory for polymers grafted on a non-adsorbing surface using the following equations:

$$R_F = aN^{3/5} \tag{3}$$

$$L = aN(a/D)^{2/3} \tag{4}$$

where R_F is the Flory radius, N is the degree of polymerization, a is the monomer size, D is the distance between grafting points of polymers in the lateral plane, and L is the thickness of the brush-like polymer layer. Therefore, for PEG with M_w of 5 kDa, $N = 113.6$, the monomer size is 0.35 nm, thus $R_F \sim 6$ nm. Moreover, considering the experimentally obtained footprints of 13.7 nm^2 and 17.5 nm^2, the thickness of the polymer grafted onto Au NRs, L, are 12.2 nm and 11.2 nm for PEG-COOH and PEG-NH_2, respectively. Based on the above and according to the experimental results of size increase, the grafted PEG chains in both cases lay between the mushroom- and brush-like regimes, but as mentioned previously and in any case, not in a fully stretched conformation [40].

It is also important to bear in mind that surface curvature plays an important role on defining PEG's grafting density [41,42], and that the geometry Au NRs combines regions with high surface curvature, at the nearly spherical ends, and lower surface curvature at the cylindrical region, and that surface curvature strongly influences the conformation of PEG chains in an intermediate grafting regime; thus, the grafting density in Au NRs might also be heterogeneous depending on the geometric region of the nanostructures. On the other hand, partial and heterogenous PEGylation can be inferred from the shift of the LSPR peak, where blue-shifts (like the one observed for PEG-COOH coated Au NRs, Fig. 1d) are known to be originated from side-on aggregation whereas end-on-end aggregation would cause a red-shift [43]. Thus, an hypsochromic shift could be ascribed to a preferential PEGylation at the ends of the Au NRs, contrasting with the higher curvature conjecture. Based on the above, the complexity of the ligand exchange process in CTAB-synthesized Au NRs becomes obvious, and with the current experimental evidence we can assume that PEG is not necessarily homogeneously distributed in the available surface; this could affect, in consequence, the protein adsorption on the Au NR's surface.

Both types of PEG-coated Au NRs were colloidally stable for long times (weeks) without appreciable changes in both particle hydrodynamic diameter and ζ-potential values (Fig. 1g); only a very slight reduction in surface charge was observed for PEG-COOH-coated Au NRs at the beginning of the incubation process probably consequence of some electrostatic screening of dissolved ions in solution when forming the particle electric double layer [44].

3.2. Determination of protein-Au NRs interactions and bioconjugate formation

For intended biomedical applications, the interactions between proteins existing in the biological environment and NPs are key since these can alter/modify the properties, colloidal stability and intended biological fate of the latter [45,46]. For such a reason, a deep knowledge about such interaction and the potential bioconjugates that can be formed is essential to optimize NP design and function.

Here, the evolution of the Au NR-protein interactions and subsequent adsorption of BSA and FIB molecules onto the different types of functionalized Au NRs (CTAB, PEG-COOH and PEG-NH_2) to give Au NR-protein bioconjugates was evaluated. BSA and FIB are structurally different proteins: BSA possesses a heart-lobe structure, with a molecular weight of 66 kDa and dimensions $4 \times 4 \times 14$ nm^3, which correspond to the prolate-like shape of this protein in water; meanwhile, FIB is a soluble plasma glycoprotein which is converted by thrombin into fibrin during blood clot formation. It has a molecular weight of 340 kDa with a

cylindrical morphology with dimensions of 45 × 5 × 5 nm^3, and comprises of pairs of α-, β-, and γ-chains, each containing 562, 461, and 411 amino acid residues, forming three domains [47]. It is also worth mentioning that the achievement of a permanent and stable protein corona usually formed by a "hard" layer of slowly exchanging protein(s) and an outer, more loosely bound layer (the so-called "soft" corona) is time-dependent [48, and a purification process is required to distinguish whether the adsorbed proteins were in equilibrium with the free proteins in solution, or they were irreversibly bound forming a stable protein corona determining the identity of the protein-NP bioconjugate.

UV–Vis spectral changes of CTAB, PEG-COOH and PEG-NH_2-coated Au NRs upon incubation with BSA and FIB in the range of 0–2.0 and 0–0.4 μM, respectively, denoted the existence of interactions between the metallic NPs and both proteins, as observed in Fig. 3. For CTAB-coated Au NRs there exists a progressive red-shift up to values of ca. 7 and 15 nm upon incubation with BSA and FIB, respectively (Fig. 3), which denotes the formation of a denser dielectric layer onto the Au NR surface consistent with the adsorption of proteins; hence, a protein corona is formed. In addition, a certain broadening in the LPSR band is also observed which probably also reflects the potential formation of some protein-NP clusters, as corroborated by DLS population distributions (see below). In this regard, it is known that BSA and FIB molecules are negatively charged at neutral pH (their isoelectric points are 5.6 and 5.8, respectively) [49], whereas CTAB-coated Au NRs are electrically positive. Thus, the observed broadening might be ascribed to certain particle clustering induced by both proteins as a result of electrostatic interactions between the proteins and the CTAB-coated metallic NPs. Conversely, for both types of PEG-coated Au NRs the broadening observed in the UV–Vis absorption spectra upon incubation with both proteins is smaller, with red-shifts of ca. 7 and 4 nm for PEG-COOH-coated AuNRs (Fig. 3b-e), and 10 and 5 nm for PEG-NH_2-coated ones when BSA and FIB are adsorbed, respectively (Fig. 3c-f). In addition, it is worth mentioning that the formation of a perfectly stable protein corona needed a certain time to be fully developed (ca. 2 h) in agreement with previous works [18,50].

Population size distributions of BSA interacting with the different types of functionalized Au NRs (Fig. 4a-c) confirmed the presence of two peaks corresponding to the diffusion modes of the metallic NPs at ca. 2–3 and 40–50 nm. A progressive shift of the maximum of the distribution corresponding to the translational diffusion mode to larger hydrodynamic diameter, $D_{h,app}$, took place upon interaction of this protein with CTAB-coated Au NRs. For this type of metallic NPs a certain broadening of the population size distribution compatible with the formation of dense protein layer(s) which gives rise to larger-sized bioconjugates was observed; nevertheless, the formation of some bioconjugate clusters cannot be disregarded; in addition, the appearance of some additional peaks at sizes between 1 and 10 nm that might be related also to the existence of some protein oligomers in solution. The latter peaks are not observed upon interaction of BSA with PEG-NH_2-coated Au NRs, for which only the rotational and translational diffusion population modes were discerned, being the latter slightly shifted to larger $D_{h,app}$ as the protein concentration in solution increases, which is compatible with the corona formation despite the presence of the antifouling oxyethylene groups. In the case of FIB, similar patterns were discerned (Fig. 4d-e), that is, interactions of FIB with CTAB-coated Au NRs led to larger $D_{h,app}$ values with evident signs of particle clusters in solution; meanwhile, for PEG-NH_2-coated Au NRs changes are much smoother and only two population modes were present.

On the other hand, special mention deserves the interaction of BSA and FIB with PEG-COOH-coated Au NRs. The formed bioconjugates showed very stable hydrodynamic size populations (Fig. 4c,f). These results seem to confirm the role played by negatively charged coating layers, which stabilized the NPs against large-scale aggregation probably by precluding strong interactions with the proteins in solution, giving rise to a less dense protein corona. In summary, the aggregation behavior of Au NRs is, then, confirmed to have an intimate relationship with the type of capping ligand and the surface charges [6,8,10].

A first rough estimation of the thickness of the formed protein corona

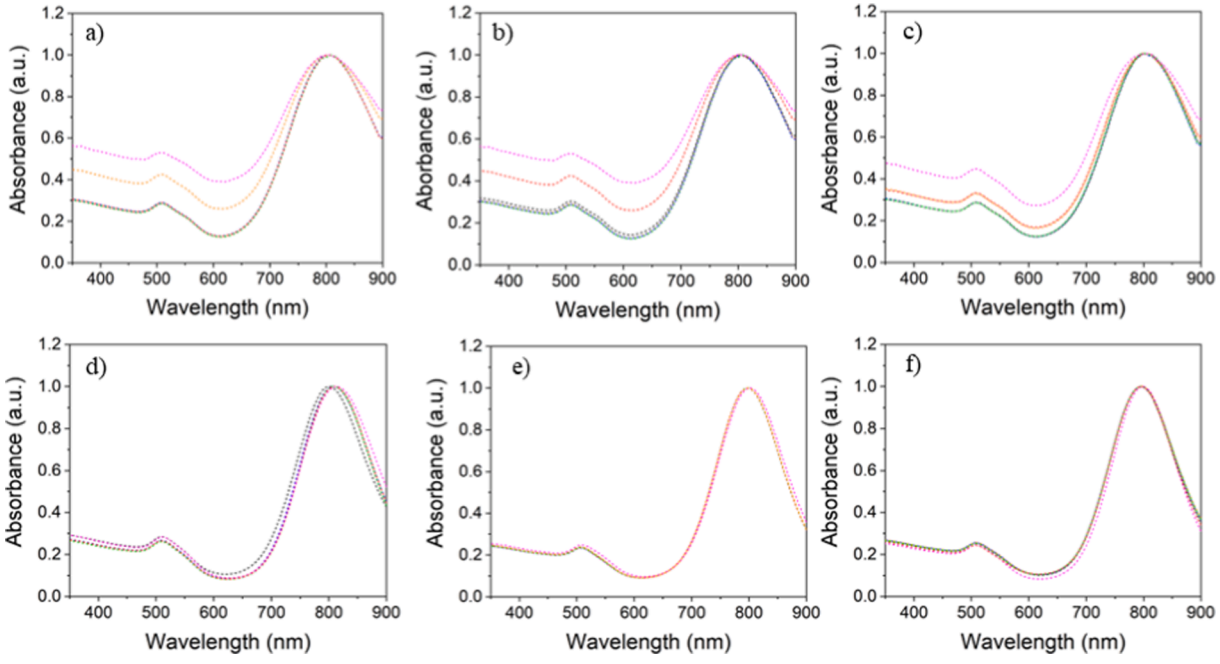

Fig. 3. UV–visible spectra absorption upon interaction of BSA (a-c) and FIB (d-f) with CTAB- (a,d); PEG-COOH- (b,e) and PEG-NH_2- (c,f) coated Au NRs. The concentrations of BSA were (—) 0; (——) 0.2; (——) 0.4; (——) 1.0; (——) 1.6 and (——) 2.0 μM, and that of FIB was (—) 0; (——) 0.03; (——) 0.05; (——) 0.1; (——) 0.2 and (——) 0.4 μM. All measurements were carried out in PBS (0.01 M, pH 7.4) at 25 °C.

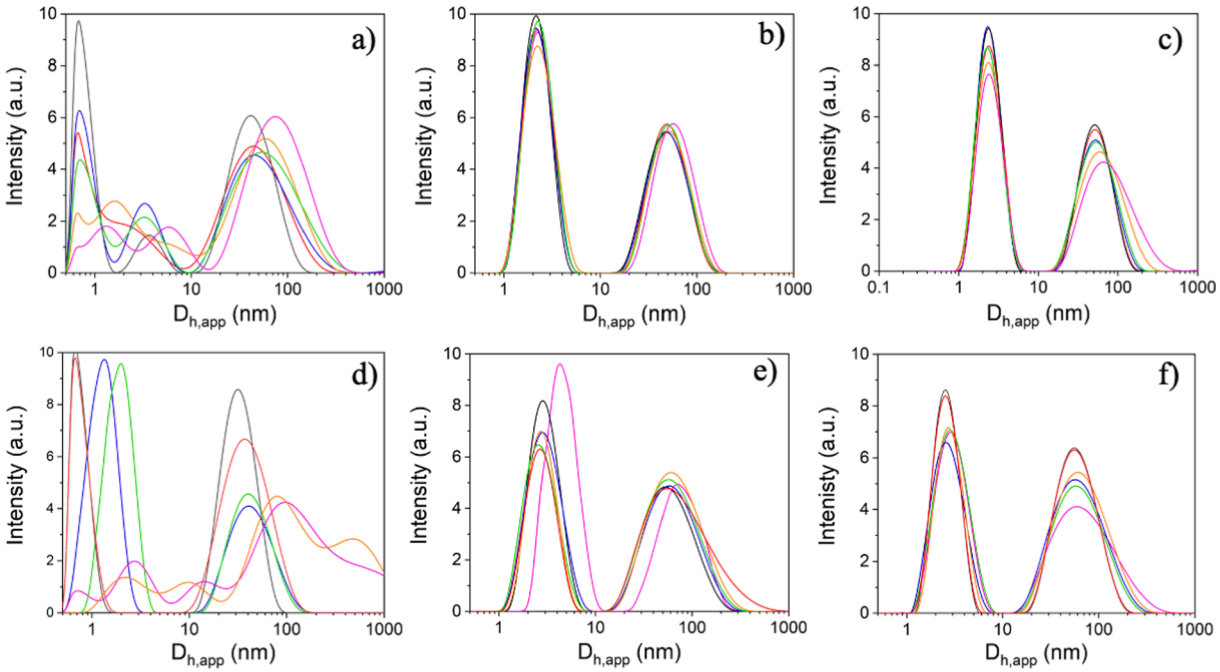

Fig. 4. Population size distributions obtained by DLS for BSA (a-c) and FIB (d-f) in the presence of CTAB- (a,d); PEG-COOH- (b,e) and PEG-NH_2- (c,f) coated Au NRs at different NP concentrations: (—) 0; (—) 0.2; (—) 0.4; (—) 0.8; (—) 1.0 and (—) 2.0 μM.

after BSA and FIB adsorption onto the different types of Au NRs was obtained from DLS data by comparing the particle hydrodynamic sizes before and after protein adsorption (translational diffusion mode). In this manner, it was found that the effective "size" of PEG-NH_2-coated and, particularly, CTAB-coated Au NRs increased as BSA and FIB were adsorbed onto the NPs surfaces. In this manner, corona thicknesses of ca. 18 and 20, and 6 and 7 nm were noted for CTAB-coated and NH_2-coated Au NRs upon interaction with BSA and FIB, respectively (see also Table 1). The data for CTAB-coated Au NRs would be compatible with the formation of either a protein multilayer surrounding the NPs (the approximate hydrodynamic diameters of both BSA and FIB are ca. 7.0 [51] and 12.7 nm [47], respectively, under the assumption of spherical geometry) and/or the formation of bioconjugate clusters, the latter actually consistent with the redshifts observed in the plasmon absorption band of CTAB-coated-Au NRs underwent in the presence of the proteins; on the other hand, for PEG-NH_2-coated Au NRs the observed hydrodynamic size increase would be compatible with the development of a single adsorbed protein layer. Conversely, the protein corona on the surfaces of PEG-COOH-Au NRs appeared to be smaller, ca. 4 nm as measured by DLS for both BSA and FIB, which might indicate that the surface of this type of metallic NP might not be completely coated with protein molecules. This would agree with the stealthiness provided by the PEG backbone but also by the small but negative electric charge of this type of PEG polymer playing, thus, an important role in providing some repulsive interactions with proteins. Finally, changes in zeta potential data of the different functionalized Au NRs upon interactions with oppositely charged protein residues also confirmed the adsorption of BSA and FIB molecules onto the different types of Au NRs (Table 1).

Table 1
Changes in NP mean hydrodynamic sizes and ζ-potentials upon protein adsorption, and estimation of the number of adsorbed protein molecules (N) by fluorometric and Bradford assays.

Bioconjugate	$\Delta D_{h,app}$ (nm)	Δζ [1] (mV)	N (Fluorescence)	N (Bradford)
BSA				
CTAB-Au NRs	18 ± 5	−34.1 ± 8.6	75 ± 9	85 ± 12
PEG-COOH-Au NRs	4 ± 1	+5.4 ± 2.7	11 ± 4	18 ± 5
PEG-NH_2-Au NRs	6 ± 2	−10.3 ± 3.1	34 ± 7	44 ± 9
FIB				
CTAB-Au NRs	20 ± 6	−35.2 ± 9.7	27 ± 6	30 ± 7
PEG-COOH-Au NRs	4 ± 2	+4.7 ± 1.8	10 ± 3	14 ± 4
PEG-NH_2-Au NRs	7 ± 3	−27.0 ± 7.1	15 ± 3	18 ± 3

[1] Negative values indicate a reduction in positive ζ potentials, whereas positive ones reflect the opposite trend (increases in negative values).

It was observed that the formed Au NR-protein bioconjugates were stable in solution for long periods of time even though in some cases ζ-potential values were below the thresholds needed to prevent particle aggregation by means of electrostatic repulsions (ca. ± 30 mV); thus, this fact clearly indicated that particle colloidal stability was also mediated by steric repulsions between the adsorbed protein molecules and PEG-coated NPs, which helps to preserve their physico-chemical properties.

The degree of protein surface coverage of the Au NRs is also an important parameter that provides information whether a sparse or a dense layer of protein was formed onto the particle surfaces, even if multiple layers may be present. Calculation of the maximum number of protein molecules onto the Au NRs was performed by calculating the surface area of the NPs (considering the geometrical dimensions of Au NRs derived from TEM) at half a protein diameter above the particle and divided by the protein cross section as previously described [18]. For simplicity, BSA was considered as having a spherical shape with a mean diameter of 7 nm with calculated cross-sectional area of ca. 38,5 nm^2, whereas FIB was considered as a cylinder of 45 nm long and 5 nm width and approximate end-on and side-on cross-sectional areas of 35 and 128 nm^2 [52]. Therefore, the maximum number of protein molecules in a monolayer surrounding an Au NR would be then, ca. 66 for BSA, and 9 and 60 for FIB in a side-on and end-on configuration, respectively.

The number of adsorbed BSA and FIB molecules per CTAB, PEG-COOH and PEG-NH_2-coated Au NRs (2 nM) was experimentally estimated by means of protein quantification in supernatants by fluorescence measurements using FITC-labeled proteins and the Bradford protein assay, respectively, after incubation of the metallic NPs in the

presence of 5.0 μM of BSA and 1.0 μM of FIB, respectively. Comparison with theoretical data confirms that only for CTAB-coated Au NRs a full BSA monolayer is formed, whereas for the remaining cases (PEG-coated Au NRs in the presence of both BSA and FIB, and CTAB-coated Au NRs in the presence of FIB) protein adsorption, under the performed incubation conditions, gave rise only to a partial coverage of the NP surfaces.

Table 1 shows that CTAB-Au NRs adsorbed more protein molecules than PEG-NH_2-ones in agreement with UV–Vis and DLS data, probably consequence of the larger positive surface electric charge, hydrophobicity, and the lack of steric hindrance provided by the polymer chains in PEGylated AuNRs; in fact, for PEG-COOH-coated Au NRs the extent of protein surface association is largely reduced probably due the coulombic repulsion between the deprotonated carboxylate groups and the overall negatively charged proteins, and despite the potential interaction of the positively charged protein residues with polymeric carboxylic moieties. In addition, a larger number of BSA molecules were adsorbed onto the NP surfaces as compared to FIB. The much larger size of the latter biomolecule and its lower structural flexibility might explain the obtained results [9]. It is worth mentioning that the extent of protein coverage is dependent not only of particle and protein morphologies and available surface groups, concentrations, available surface areas, etc, but also largely influenced on the mixing conditions under which they are put into contact [53].

Despite following an improved PEGylation protocol, a low grafting density were achieved for both PEGs, thus, two possible scenarios might explain the observed protein adsorption on Au NRs. First, it is likely that either mono- or bi-layers of CTAB remain in the non-PEGylated surface of Au NRs. This persistent CTAB may have an important influence on the observed absorption of both proteins, suggesting a deficient steric hindrance provided by PEG chains; and the second surges CTAB was efficiently removed but pristine Au is available to interact with both proteins through chemisorption processes. Whatever the case, the formation of a protein corona is confirmed and a new biological identity attained.

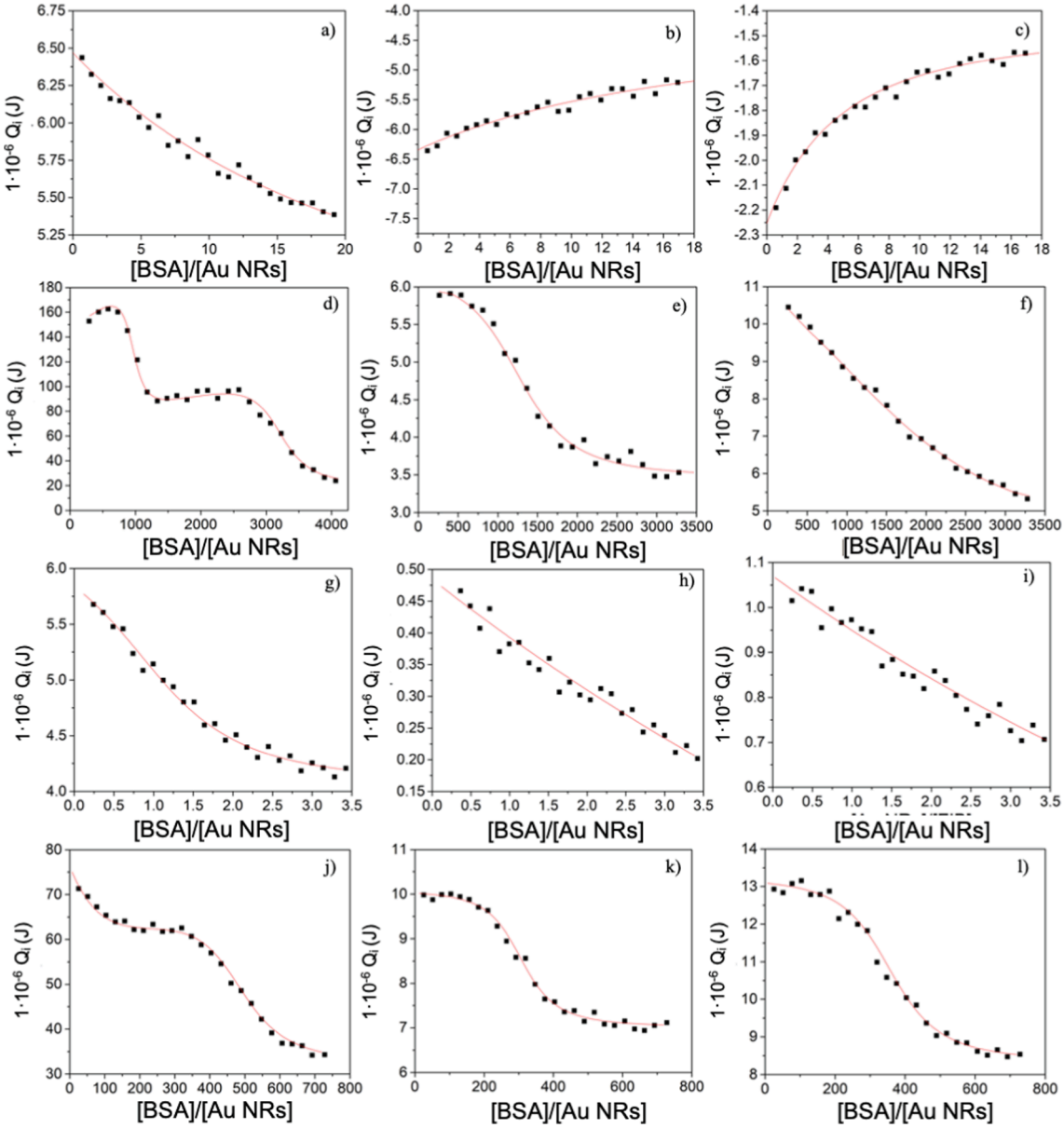

Fig. 5. ITC data from titration of (a-f) BSA and (g-l) FIB onto (a,d,g,j) CTAB-; (b,e,h,k) PEG-COOH-, and (c,f,i,l) PEG-NH_2-coated Au NRs upon injection of 0.17 and 36 μM of the former protein, and 0.034 and 7.2 μM of the latter. The red lines correspond to the fits. (For interpretation of the references to colour in this figure legend, the reader is referred to the web version of this article.)

3.3. Thermodynamics of protein-Au NRs binding

To quantify the relative strength of Au NRs-BSA and FIB interactions and their dependence with their selected surface coating and protein type and structure, the equilibrium binding constant K and the related thermodynamic quantities of the protein binding process (enthalpy, ΔH, entropy, ΔS, and Gibbs free energy, ΔG, changes and the binding stoichiometry, n_i, where i refers to the type of binding site) were obtained from isothermal titration calorimetry experiments. To completely understand the magnitude of the protein-Au NR binding interactions, the following factors must be taken into account: i) the geometrical accommodation of the protein molecules onto the NP surface, and ii) the chemical interactions between the proteins and the Au NR surface, which directly affects the protein-Au NR bioconjugate formation process. Also, it is necessary to bear in mind that the limiting factor for protein corona formation is the available Au NR surface and not protein depletion since even the less abundant serum proteins in blood are at high enough concentrations (the concentration of BSA in blood plasma is in the range of 522.4 – 671 μM [54], and that of FIB is in the range of 4.41 – 11.76 μM [55]) to coat all possible available NPs considering that their concentrations are expected to be rather diluted.

Selected curves for BSA and FIB titrated with different protein stock solution concentrations, 0.17 and 36 μM for BSA, and 0.034 and 7.2 μM for FIB, respectively, that is, protein:Au NRs molar ratios ranging from ca. 3.5 up to ca. 4000, into CTAB-, PEG-COOH, PEG-NH_2-coated Au NRs solutions are shown in Fig. 5. Upon interaction with BSA, CTAB-coated Au NRs showed endothermic decreasing profiles at both protein stock solutions tested, which denoted the progressive rupture of the NP surrounding solvation layer upon interaction with protein molecules and their subsequent adsorption (Fig. 5a,d). In particular, the heat profile at low injected protein concentrations (e.g., 0.17 μM for BSA) might be particularly affected by different processes which might simultaneously occur as, for example: i) CTAB-induced desorption from the NP surface; b) free CTAB-BSA interactions/complexation; and iii) BSA adsorption onto Au NR surface. Conversely, at a larger injected stock protein concentration (36 μM) free protein-NP surface, free protein-biocorona and free protein-free protein interactions would become more predominant since the whole, still existing loosely bound CTAB molecules located onto the NP surface would have been released to the surrounding medium [38]. Of particular interest is the presence of a shoulder with a maximum in the heat profile at ca. 3–6 μM of injected BSA onto CTAB-coated Au NRs (Fig. 5d, NP:BSA ratio between ca. 1250–2500), which can be associated with structural rearrangements of the adsorbed protein molecules to accommodate the proteins and allow the development of additional protein coating layers surrounding the NPs, in agreement with the stoichiometry values derived from the fits (see below); nevertheless, a heat contribution related to bioconjugate cluster formation might not be disregarded. However, in the protein range analyzed, no biconjugate precipitation was observed upon titration experiments.

Conversely, for both PEG-COOH (Fig. 5b) and PEG-NH_2-coated (Fig. 5c) Au NRs an initial decreasing exothermic heat profile when titrating the 0.17 μM BSA stock concentrations, in agreement with the predominance of electrostatic and/or hydrogen bonding interactions. Similar exothermic profiles were observed, for example, for the interaction of citrate-caped spherical [18,38,56–58] and polymeric NPs [48,59] with BSA, human serum albumin (HSA), fibrinogen, hemoglobin, immunoglobulin, chymotrypsin or myoglobin, for example. When titrating a 36 μM BSA stock solution the former heat flow transformed into an endothermic profile (Fig. 5e-f). It is worth mentioning that similar endothermic profiles were previously observed at very large injected BSA stock solutions [60]. This change might be associated to the fact that at relatively high added protein concentrations potential attractive electrostatic interactions between the PEG ionizable moieties (either COOH or NH_2) and the oppositely charged protein residues as well as hydrogen bonding between the polymeric chains and the protein residues would be completely offset by the effect of the hydration layer disruption (hydrogen bonding rupture) upon BSA binding; in addition, the dynamics of the protein corona, that is, the continuous exchange of adsorbed and surrounding protein molecules onto the particles, would also play an important role [48].

On the other hand, when FIB is injected into Au NRs a decreasing endothermic profile is observed for all types of functionalized NPs, in striking contrast with the observations made for BSA (Fig. 5g-l). Here, it is necessary to consider that the dimensions of FIB are comparable with those of the Au NRs so even at low injected protein concentrations the adsorption process might involve a very important hydration layer destabilization, thus, favoring the observed endothermic heat profiles [60]. In addition, for CTAB-coated Au NRs a similar shoulder as for BSA was observed upon injection of 0.4 μM FIB (Fig. 5j), and the associated protein rearrangement involved might be related to a progressive change from a side-on to an end-on FIB configuration, facilitating the additional adsorption of protein molecules onto the Au NRs (see below), although as in the case of BSA, heat contributions from biconjugate cluster formation cannot be disregarded.

A global examination on the thermodynamic parameters (derived by fitting the experimental data using the mode of single or double set of identical sites depending on the heat profile, see Experimental Section) listed in Table 2 reveals some interesting features. For the interaction of BSA and FIB with CTAB-, PEG-COOH- and PEG-NH_2-coated Au NRs an unfavorable enthalpy change ($\Delta H_i > 0$) is partially offset by a favorable entropy loss ($\Delta S_i > 0$), except for the titration of the low stock BSA solution concentrations into the PEG-coated NPs for which the opposite behavior was observed, that is, favorable enthalpy changes ($\Delta H_i < 0$) and unfavorable entropy ones ($\Delta S_i < 0$). Overall, the free energy changes (ΔG_i) upon protein binding were negative, confirming that the interaction is spontaneous, and ranged from − 33.5 to − 54.6 kJ mol^{-1} and −28.7 to −50.7 kJ mol^{-1} for BSA and FIB, respectively. From an enthalpic viewpoint, the formation of noncovalent bonds upon protein − NP interaction is exothermic while the disruption of structurally well-defined solvent shells is endothermic [61]. In this context, these data, in general, support the idea of an important solvent reorganization taking place upon the interactions and subsequent adsorption of protein molecules onto the NP surfaces accounting for great contributions to enthalpy changes an important favorable contributions to the entropy change associated to water desolvation, which is large enough to compensate the entropy loss due to protein freedom reduction upon binding, giving rise to overall positive entropy changes except for BSA at the titrated concentration. Only for the interaction of PEG-coated Au NRs at the low stock BSA concentrations (0.17 μM) the picture is different, and probably dominated by hydrogen bonding between the protein residues and the polymer chains. In addition, the possible existence of hydrophobic interactions between protein amino acid residues and the surfactant/polymer stabilizing particle layer can also be an important contribution to the observed positive enthalpy changes [61].

On the other hand, binding constants are in the order of 10^4–10^9 M^{-1}, similar as those previously obtained for BSA and FIB, and other proteins such as HSA, casein, transferrin, α-lactalbumin, human carbonic anhydrase II, cytochrome *c*, lysozyme, coagulation factor VII, high density lipoprotein, or chimotrypsin interacting with polymeric [48,59,62] Anozie et al., 2020, semiconductor [63], and metal NPs [18,38,56–58,64,65]. From the K_i and n_i values obtained it can be observed that the interaction of BSA to the different Au NRs is stronger than for FIB, in agreement with the larger size of the latter protein and its more rigid structure. Also, protein − Au NRs interactions become more endothermic and binding constants also increase when Au NRs are positively charged, particularly, for CTAB-coated ones at the largest protein concentration injected (36 and 7.2 μM for BSA and FIB, respectively). This fact is compatible with a larger extent in protein adsorption in agreement with the stoichiometry numbers obtained (n_i). Also, it is worth mentioning the stoichiometry values obtained by ITC are larger than the number of protein molecules bound to the NP previously obtained by fluorescence measurements. The differences may

Table 2
Thermodynamic parameters of the interactions between BSA and FIB and the different types of functionalized Au NRs.

Coated Au NRs (μM)	ΔH_i (kJ/mol)	$10^{-6}\ K_i$ (M^{-1})	ΔG_i (kJ/mol)	ΔS_i (kJ/mol)	n_i	Protein coverage[a,b]
BSA						
CTAB						
1.7	3290 ± 189	1620 ± 115	−54.6 ± 9.6	10.8 ± 2.5	33 ± 6	0.53
36	809 ± 98/ 1050 ± 256	505 ± 88 /25 ± 8	−51.8 ± 7.7/ −43.1 ± 6.1	2.8 ± 0.5/ 3.0 ± 0.3	980 ± 145/ 2254 ± 340	15.8/36.4
PEG-COOH						
1.7	−97 ± 22	1.4 ± 0.4	−36.5 ± 9.3	−0.20 ± 0.04	4 ± 1	0.06
36	70 ± 19	0.44 ± 0.11	–33.5 ± 10.5	0.33 ± 0.07	103 ± 15	1.7
PEG-NH_2						
1.7	–233 ± 35	5.3 ± 1.2	−40.0 ± 8.7	−0.62 ± 0.12	7 ± 2	0.11
36	244 ± 45	3 ± 0.6	−38.4 ± 7.1	0.91 ± 0.19	298 ± 42	4.8
FIB						
CTAB						
0.034	1240 ± 278	345 ± 66	−50.7 ± 15.1	4.15 ± 0.77	12 ± 3	4.0[a]-0.03[b]
7.2	1500 ± 401/ 1850 ± 378	145 ± 29/ 53 ± 9	−48.4 ± 8.6/ −45.8 ± 8.2	4.99 ± 1.01/ 6.11 ± 0.92	42 ± 5/ 450 ± 33	14[a]-1.2[b]
PEG-COOH						
0.34	460 ± 56	0.38 ± 0.08	–33.1 ± 7.9	1.59 ± 0.51	3 ± 1	1[a]-0.1[b]
7.2	68 ± 13	0.07 ± 0.01	−28.7 ± 5.8	0.31 ± 0.11	25 ± 6	8.3[a]-0.07[b]
PEG-NH_2						
0.034	742 ± 201	0.74 ± 0.22	−34.8 ± 7.4	2.51 ± 0.57	4 ± 2	1.3[a]-0.01[b]
7.2	207 ± 61	0.13 ± 0.04	−30.2 ± 7.1	0.76 ± 0.18	61 ± 12	20.[a]-0.17[b]

i refers to the type of binding sites: $i = 1,2$ (first class and second class where corresponding, that is, for CTAB-coated Au NRs and the largest stock BSA and FIB stock concentrations injected).
[a] FIB adsorbed in a side-on configuration.
[b] FIB adsorbed in an end-on configuration.

arise from the different conditions used for the experiments (fixed protein:NP ratio in fluorescence measurements and a dynamic one in ITC ones) as well each technique may be affected by different constraints: In fluorescence, the measurement of the adsorbed protein concentration is indirect, and the potential presence of some remaining bioconjugate in the supernatant might alter somehow the measurement; meanwhile, in ITC other processes than the protein-NP interaction as protein–protein complexation and/or bioconjugate clustering may be also taking place, thus, contributing to the heat profile.

Considering the maximum number of protein molecules in a monolayer surrounding the Au NR surface and the stoichiometry values, the total surface coverage of the NPs was obtained. It was observed that the surface coverage was larger for the cationically charged Au NRs and slightly more important for BSA than FIB, probably as a result of the larger size of the latter biomolecule. From the surface coverage values, a protein multilayer would seem to be developed on the cationically NP surfaces, particularly for CTAB-coated Au NRs. In addition, from the data to accommodate this biomolecule on the surface of CTAB-coated Au NRs a transition to a protein end-on configuration would be required, in agreement with the observations made. In contrast, PEG-coated NPs would be able to accommodate FIB in a side-on configuration when injected the most diluted protein concentration, and a coexistence of both modes of adsorption might take place at larger injected stock concentrations, still allowing free particle surface for additional protein adsorption. Previously, it has been shown that FIB tends to be adsorbed on small-sized gold (5.6–14 nm) and silica (15–60 nm) NPs via side-on configuration [29,66]; however, FIB preferably attached to NPs surface through end-on configuration as the size of NPs increased [56]. Nevertheless, and as mentioned above, these data should be taken as a bare approximation provided the inherent assumptions present in the fitting model and other processes than protein:NP interactions may take place in parallel.

3.4. Structural conformation of protein corona

The protein corona may help Au NRs to act as a "trojan horse" allowing their deeper penetration into cells and tissues. Since protein-coated NPs are the biologically relevant entity, any change in their composition, concentration, conformation, and/or packing of the adsorbed layer(s) surrounding the NP surfaces may affect their subsequent biological interactions with body cells and tissues. For example, BSA adsorbed on the surface of cationic polystyrene NPs experienced structural changes, while the bounds to anionic polystyrene remained intact [23]. These variations in the protein structure at the biocorona led to different interactions of the NPs with cell receptors, i.e. the BSA-coated cationic and anionic NPs bounded to scavenger and native albumin receptors, respectively. In a similar study, Minchin et al. demonstrated that silica NPs have the capability to change the albumin's structure, leading to exposure of a typical hidden epitope, which is exclusively recognized by macrophages expressing class A receptor [13,67]. Prapainop *et al.* also demonstrated that apolipoprotein conformation was changed after binding to quantum dots substantially increasing their uptakes by macrophages [5]. In addition, the conformation of the adsorbed proteins takes special relevance due to the potential risk of decreasing the NPś *in vivo* functionality or initiating a series of cascade reactions associated to protein misfolding and denaturation processes originating either disease and/or toxicity [2,5,15,68]. For instance, structural changes in fibrinogen (i.e., exposure of its C-terminous of γ chain ($\gamma^{377–395}$), after interaction with poly(acrylic acid)-coated gold NPs, can provoke the inflammation response and downstream unwanted cascade pathways [29].

To additionally confirm the existence of interactions between the different types of Au NRs and both BSA and FIB as well as gaining initial knowledge about the potential conformation of these proteins on the Au NRs surfaces, that is, when forming the protein corona, NP concentration-dependent fluorescence spectroscopy measurements were performed by taking advantage of the efficiency of gold-induced fluorescence quenching of protein chromophores, which reveal useful information about the relative accessibility of Au NRs to hydrophobic protein residues and pockets. The efficiency of this fluorescence quenching depends on the distance between the quencher and the chromophore [69]. In this regard, it is necessary to remind that BSA contains two tryptophan groups, -Trp134 placed on the surface of the molecule at subdomain IB and Trp213 located at the physiologically important subdomain IIA [70], and 18 tyrosine residues along its polypeptide structure, of which only one (Tyr263) is located in

subdomain IIA [71]. Conversely, the primary structure of FIB contains a total of 72 intrinsically fluorescent tryptophan residues distributed along the molecule, with each Aα, Bβ, and γ chains having 11, 14, and 11 of these residues [72] as well as 134 tyrosines along the polypeptide, for which those two localized on the β-chain, Tyr292 and Tyr422, are involved in *in vivo* nitration which play a key role on fibrin clot formation [73]. It is important to remember that fluorescence can be enhanced depending on the distance between the fluorophore and the gold surface, therefore, we previously confirmed the lack of such effects at our experimental working conditions.

Fig. 6 show the fluorescence spectra of BSA and FIB incubated at increasing concentrations of the different types of surface-functionalized Au NRs in the range of 0 to 0.75 nM. It was illustrated that the presence of NPs causes the fluorescence intensity of both proteins to decrease, additionally corroborating the effective interactions between the particles and both proteins. This effect stems from relative alterations in the proximity between the protein chromophore and the quenching agent (the NP) as a consequence of possible changes in protein conformation/protein rearrangements upon interaction and subsequent adsorption onto the Au NRs surfaces, for example, by the exposure of internal protein chromophores typically hidden in the folded state [51,74].

Furthermore, it can be also observed that fluorescence spectra progressively blue-shifted ca. 21 nm for CTAB-coated Au NRs upon interaction with BSA, which is consistent with changes at the protein tertiary structure level due to the burial of tryptophan residues in a more hydrophobic environment on the NP surface, thus, becoming less exposed to solvent. This would agree with the existence of stronger interactions with this type of Au NR in agreement with ITC data. In this regard, no spectral shifts were observed for PEG-COOH and PEG-NH_2 Au NRs, in agreement with their relatively lower binding affinity for the proteins as commented above (see above) A similar behavior can be also observed when FIB is interacting with CTAB-, PEG-COOH- and PEG-NH_2-coated Au NRs. The larger stiffness of FIB would slightly reduce the amount of surface adsorbed protein molecules, in agreement with the observed some smaller fluorescence quenching ability and the lower binding constants and stoichiometries obtained previously by ITC.

The fluorescence quenching mechanism was also evaluated using the Stern-Volmer equation:

$$\frac{F_0}{F} = 1 + k_q \tau_0 [Q] = 1 + K_{SV}[Q] \quad (5)$$

where F_0 and F are the fluorescence intensities of proteins in the absence and presence of the quencher (Au NRs); k_q and K_{SV} are the biomolecular quenching rate constant and Stern–Volmer quenching constant, respectively; [Q] is the quencher concentration; and τ_0 represents the average lifetime of an excited biomolecule without a quencher ($1.0 \cdot 10^{-8}$ s [66]. It was found that K_{SV} could be determined by a linear regression of a plot of $\frac{F_0}{F}$ against the quencher [Q], that is, the Au NRs in the range of lower concentrations (Fig. 6g-h). The Stern–Volmer quenching constants Ks_V and quenching rate constants k_q for all of the interacting AuNRs-BSA and AuNRs-FIB bioconjugates are listed in Table 3. It was observed that the quenching rate constants (k_q) were greater than the limiting diffusion collision rate constant values of biomolecules (k_d, the representative value is 2×10^{10} L·mol^{-1} s^{-1}), which revealed that certain static quenching may occur when BSA or FIB bind to CTAB-, PEG-COOH- and PEG-NH_2-modified AuNRs. The largest values (10^8–10^9 M^{-1}) of the Stern − Volmer quenching constant, K_{SV}, for CTAB-coated AuNRs confirmed the formation in this case of large particle-protein interaction surfaces, in agreement with current ITC data and previous reports [58,75–77]. It is also worth mentioning that K_{SV} is slightly larger for PEG-COOH- than for PEG-NH_2-coated AuNRs pointing to a slight more intense interactions of the former type of metallic NP with both proteins, particularly, for FIB.

In addition, the Hill equation was used to quantify the relationship between the fluorescence intensity and Au NRs concentration [78]:

$$\log\left(\frac{F_0}{F} - 1\right) = \log K_a - m \log[Q] \quad (6)$$

where K_a is the association constant. The Hill coefficient, m, describes the cooperative effect of protein (ligands) molecules binding to the Au NR surface. The association constant K_a gives a rough idea about the relative rates in the competitive adsorption process when NPs are introduced the medium. As seen in Table 3 the Hill coefficient was only lower than 1 for PEG-COOH-coated Au NRs interacting with BSA, which suggests a negative cooperative binding interaction, that is, the interaction between the metallic NPs and BSA molecules became progressively weaker as additional proteins are adsorbed onto the particle surfaces. Conversely, for the other bioconjugates the binding appeared to be a positive cooperative interaction ($m > 1$), which involved that the established interactions between the proteins and the NPs led to further adsorption of protein molecules as interaction proceeds. Moreover, it was determined that the binding is more cooperative for FIB than for BSA as denoted by the slightly larger values of m, which might be related to a progressive change from a side-on to an end-on configuration of the adsorbed protein molecules onto the particle surface, in agreement with obtained values of adsorbed FIB molecules onto the particle surfaces and previous works [56,79,80].

Additional information about the potential conformation changes upon the adsorption of protein molecules onto the different types of Au NRs was gained by both FTIR and CD spectroscopies. The potential conformational change of both BSA and FIB upon interaction with Au NRs was elucidated by analyzing the changes in the protein amide I band between 1700 cm^{-1}–1600 cm^{-1} (mainly C = O stretching) and amide II one at ca. 1600 cm^{-1}–1500 cm^{-1} (C-N stretching coupled with a N–H bending mode), both related to the secondary structure of proteins. The amide I band contained contributions from different secondary structural elements, for example, from 1620 to 1645 cm^{-1} corresponds to β-sheets, from 1645 to 1652 cm^{-1} to random coils content, and from 1652 to 1662 cm^{-1} from α-helices, respectively.

FTIR spectra of BSA (2.0 μM) and FIB (0.4 μM) in the absence and presence of the different types of Au NRs are shown in Fig. 7. Some changes in peak shape and position of the amide I peak were observed for the bioconjugates as compared with that of the native proteins, which suggests the occurrence of limited changes in protein secondary structure upon protein − NP surface interactions. In the absence of the NPs, the predominant band centered at ca. 1652 cm^{-1} denotes the significant α-helix content of BSA [81]. It was observed that upon BSA adsorption, the peak of the amide I slightly decreased in intensity and progressively shifted from 1652 cm^{-1} to 1651, 1649 and 1642 cm^{-1} whereas the amide II moved from 1548 cm^{-1} to 1550, 1550 and 1553 cm^{-1} for PEG-COOH-, PEG-NH_2- and CTAB-coated Au NRs (Fig. 7a). This suggested that the secondary structure of BSA was slightly altered when interacting and adsorbed onto the two types of PEG-coated metal NPs and it is particularly strong for CTAB-coated ones, for which a transition to an unordered structure occurs (see below for additional information). On the other hand, there was no obvious change in the FTIR spectra of BSA in the presence of PEG coated-Au NRs, which confirmed a relatively low influence on this type of NPs on BSA conformation, which might be directly related to the stealth properties of the coating.

In the case of FIB, rather similar observations were noted. For the amide I and II bands a shift from ca. 1651 cm^{-1} to 1649, 1645 and 1643 cm^{-1} whereas the amide II moved from 1546 cm^{-1} to 1547, 1547 and 1555 cm^{-1} for PEG-COOH-, PEG-NH_2, and CTAB-coated Au NRs, respectively (Fig. 7b). It is worth mentioning that for CTAB-coated Au NRs the amide I band broadens to shorter wavenumbers indicating the development of unordered secondary structure whereas the amide II largely vanishes, confirming the loss of secondary structure.

This behavior was further confirmed by CD spectroscopy measurements, and the changes in protein secondary structure composition

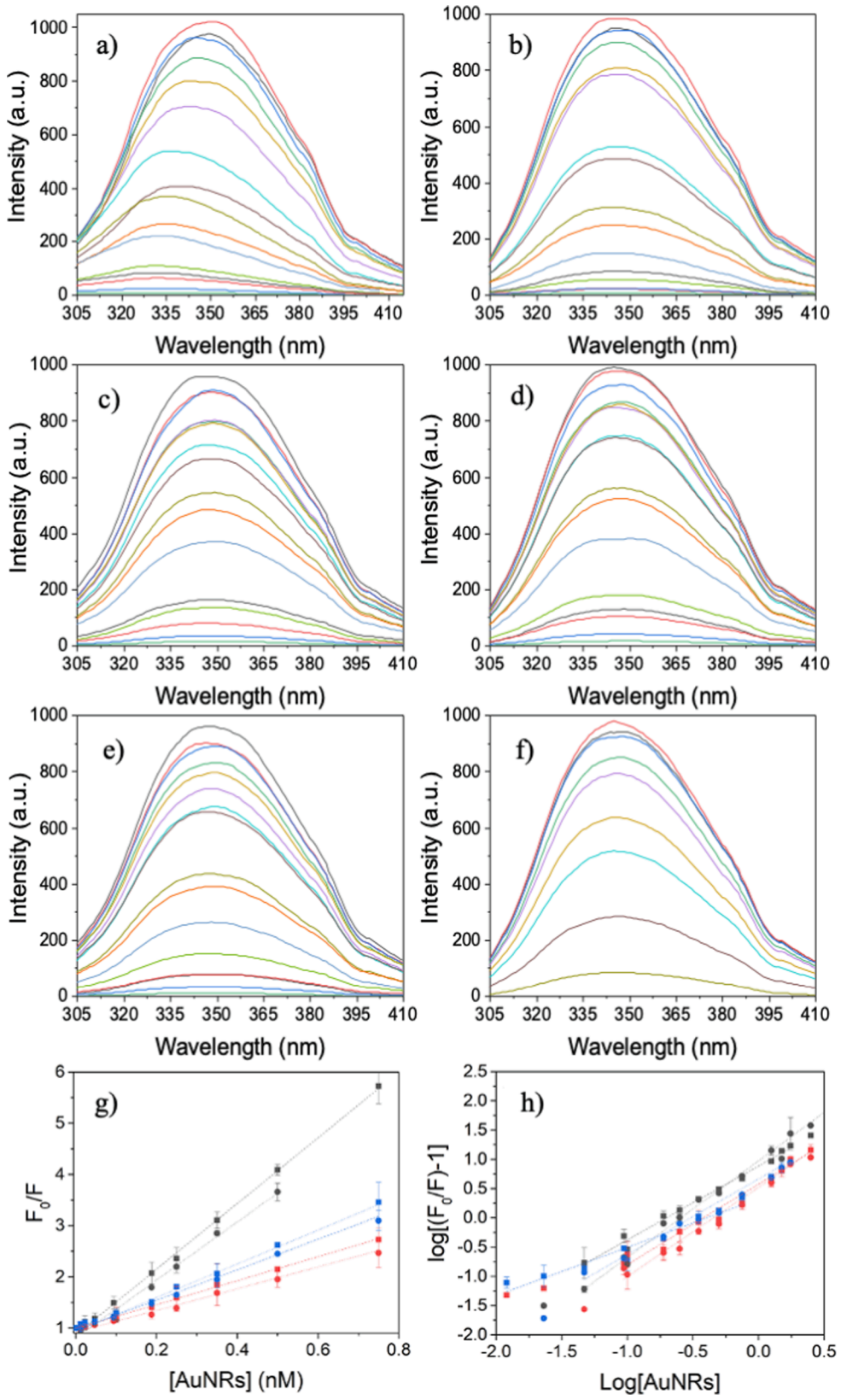

Fig. 6. Progressive fluorescence quenching of (a,c,e) BSA (2 μM) and (b,d,f) FIB (0.4 μ) upon interaction with CTAB-coated (a-b), PEG-COOH- (c-d), and PEG-NH_2- (e-f) coated Au NRs in the concentration range 0–0.75 nM. g) Stern-Volmer and h) Hill plots of the different bioconjugates derived from fluorescence data: (■) CTAB-coated Au NRs/BSA; (●) CTAB-coated Au NRs/FIB; (■) PEG-COOH-coated Au NRs/BSA; (●) PEG-COOH-coated Au NRs/FIB; (■) PEG-NH_2-coated Au NRs/BSA; (●) PEG-NH_2-coated Au NRs/FIB.

Table 3
The Stern–Volmer quenching constants *Ksv* and quenching rate constants k_q for the different AuNRs-protein systems at 25 °C.

System	10^{-9} K_{SV} ($L \cdot mol^{-1}$)	10^{-18} k_q ($L \cdot mol^{-1}$)	10^{-12} K_a (mol/L)	*m*
CTAB-AuNRs/BSA	6.41 ± 0.14	6.41 ± 0.14	1.84 ± 0.26	1.26 ± 0.04
PEG-COOH-AuNRs/BSA	2.47 ± 0.10	2.47 ± 0.10	0.94 ± 0.13	0.92 ± 0.09
PEG-NH_2-AuNRs/BSA	2.77 ± 0.19	2.77 ± 0.19	0.55 ± 0.06	1.18 ± 0.13
CTAB-AuNRs/FIB	5.66 ± 0.33	5.66 ± 0.33	1.60 ± 0.06	1.65 ± 0.06
PEG-COOH-AuNRs/FIB	1.29 ± 0.16	1.29 ± 0.16	1.28 ± 0.06	1.29 ± 0.08
PEG-NH_2-AuNRs/FIB	2.13 ± 0.10	2.13 ± 0.10	1.54 ± 0.06	1.53 ± 0.08

derived from the experimental data using suitable protein databases. Fig. 7c-d reveals the CD spectra of BSA and FIB in the presence of various concentrations of the different Au NRs. The CD spectra of both native BSA and FIB exhibited two negative absorption bands in the UV region, at 208 nm and 222 nm, showing their characteristic and predominant α-helix content. The ellipticity values of both proteins at these wavelengths increased in the presence of Au NRs and their minima progressively shifted to slightly longer wavelengths, which is direct evidence of conformational changes undergone by both proteins upon interactions with the metallic NPs. It was inferred that the conformational changes of protein molecules may have originated from the unfolding of polypeptide chains or the evolution to other type of secondary structure (e.g., β-sheets) as occurred, for example, in fibrillation processes [82,83]. The percentage of each type of secondary structure of FIB and BSA adsorbed onto the NPs at two different particle concentrations (0.5 and 5 nM) analyzed was derived from CD data using the corresponding software.

Table 4 shows that the α-helix content was modified, which demonstrated that conformational changes of both proteins were induced to a certain degree by Au NRs and enhanced with NP concentration. In addition, such rearrangements were more pronounced upon protein interaction with CTAB-coated Au NRs in agreement with FTIR data, with progressive reductions in α-helices and relatively important increases in unordered conformation and β-structures as the NP concentration increased. Furthermore, it was noted that the α-helix content of both BSA and FIB was also modified to smaller extents upon interaction with PEG-modified Au NRs as compared to CTAB-coated ones, particularly when interacting with BSA, in agreement with the lower protein adhesion to this type of coating capability as well as the lower binding affinity, which favor to keep better the protein secondary structure. It is also worth mentioning that conformational changes were slightly larger for FIB than for BSA, in agreement with other previous observation made for both proteins upon interaction with, for example, graphene oxide [84], or silica nanoparticles [66,85]. Then, it is suggested that the surface properties of Au NRs, such as surface charge, may have significantly affected conformational changes in the adsorbed proteins. In summary, it seems that Au NRs coated with positively charged groups as tetraalkylammoniums in CTAB affected the

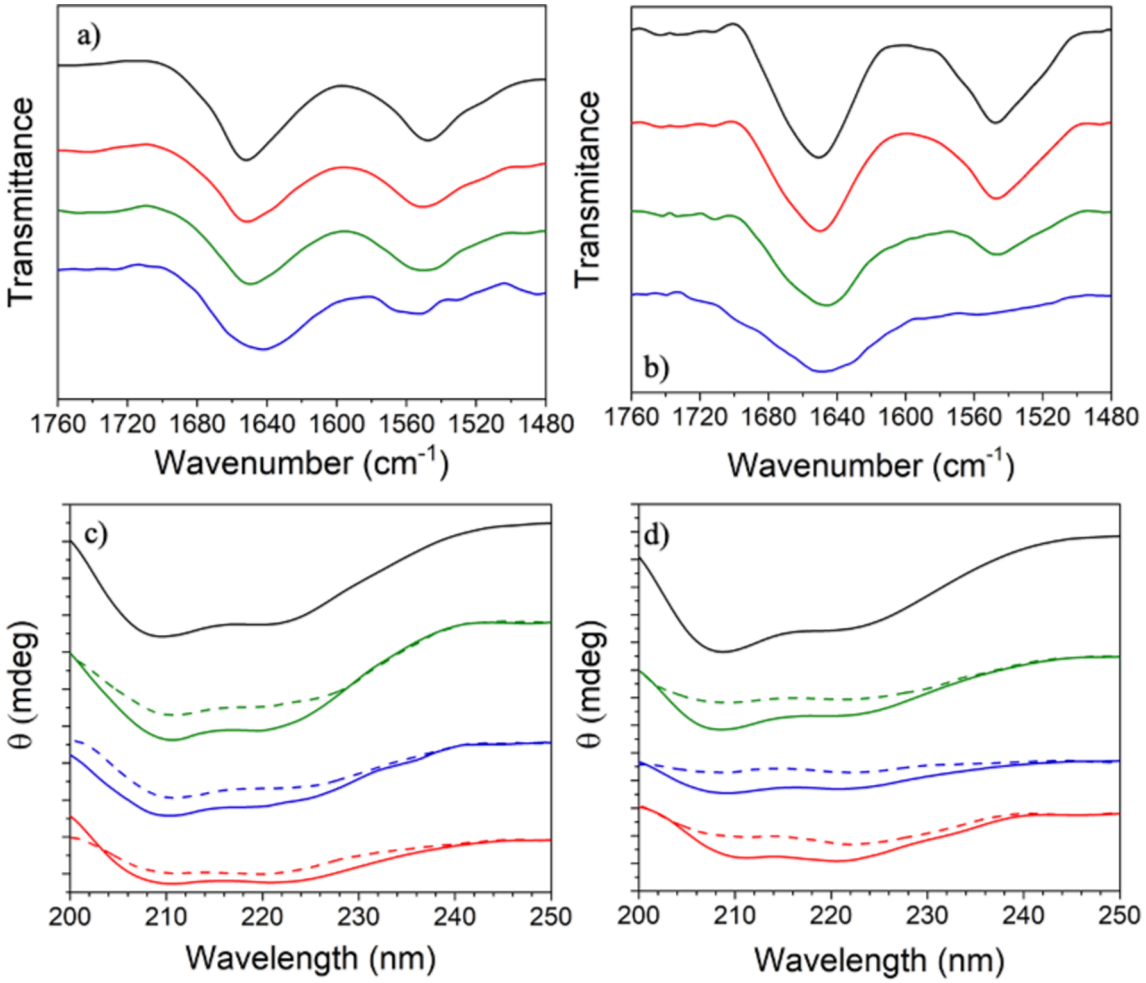

Fig. 7. a-b) FTIR and c-d) CD spectroscopy of BSA- (a,c) and FIB- (b,d) Au NR biconjugates. (—) Free protein; (——) PEG-COOH-; (——) PEG-NH_2-; and (——) CTAB-coated Au NRs.

Table 4
Percentages of secondary structure obtained from CD data for BSA and FIB proteins upon interaction with the different types of Au NRs.

System	%α-helix	%β-sheet	%β-turn	% unordered
BSA				
Pure BSA	64.9	7.2	9.2	18.7
CTAB-AuNRs (0.5 nM)	44.3	10.7	13.4	31.6
CTAB-AuNRs (5 nM)	28.1	20.5	10.8	41.6
PEG-COOH-AuNRs (0.5 nM)	60.5	8.5	10.3	21.7
PEG-COOH-AuNRs (5 nM)	48.5	9.5	11.1	29.9
PEG-NH_2-AuNRs (0.5 nM)	55.0	10.2	10.0	26.8
PEG-NH_2-AuNRs (5 nM)	41.5	12.2	10.6	35.7
FIB				
Pure FIB	57.5	8.5	12.0	22.0
CTAB-AuNRs (0.5 nM)	34.1	12.1	16.0	37.8
CTAB-AuNRs (5 nM)	20.4	20.7	15.0	43.9
PEG-COOH-AuNRs (0.5 nM)	52.3	10.2	13.1	24.4
PEG-COOH-AuNRs (5 nM)	42.6	11.7	14.2	31.5
PEG-NH_2-AuNRs (0.5 nM)	46.8	11.3	14.8	27.9
PEG-NH_2-AuNRs (5 nM)	30.3	15.3	15.0	39.4

conformational stability of adsorbed proteins to a greater extent than surface PEG chains despite the presence of charged/ionizable groups at the polymeric ends. These observations confirmed that the type of capping ligand as well as the surface particle charge of the NPs likely played an important role in the interactions of NPs with proteins.

4. Conclusions

In this work, Au NRs were successfully PEGylated with two PEGs bearing different terminal groups which confer them distinct electrical charge, and which provide a relatively low-density coverage due to the large affinity of CTAB molecules which form a bilayer to the surface of the metallic NPs. The polymeric chains at the particle surface are in an intermediate conformation between the mushroom- and brush-like regimes, as observed from DLS data. PEGylation also reduces the extent of protein adsorption by diminishing the interactions between the proteins and the anisotropic metallic NPs compared to the as-synthesized Au NRs coated with CTAB. Based on spectroscopic plasmon-shift analysis, DLS and ζ-potential, we confirm that PEG-COOH provides the highest stealthiness in PBS at physiological pH, as compared to CTAB and PEG-NH_2. However, a protein corona is still formed onto PEGylated NRs, which is even complete at large protein concentrations, as observed from ITC data for both BSA and FIB, and which involved an important disruption of the surrounding hydration layer to accommodate protein molecules, as also occurred for CTAB-coated Au NRs. Nevertheless, protein–protein interactions giving site to protein clustering and/or protein multilayer formation cannot be disregarded. Except in the case of Au NR-PEG-COOH and BSA, the adsorption of FIB and BSA to the particles seems to be a cooperative process. Importantly, FTIR and CD data confirms that the structure of proteins is altered upon interaction with Au NRs with the three types of ligands, in the following order CTAB > PEG-NH_2 > PEG-COOH. These results become relevant since the conformational alteration of protein's native structure in the corona may alter the immunogenic effects. A large body of knowledge regarding the formation of a protein corona on inorganic nanostructures and their biological implications is available, however, contradicting evidence reveals (for instance the paradigm of PEGylation) the complexity of the phenomenon, and furthermore, such inconsistencies indirectly claim for the continuity of its study, from simple and controllable conditions to more complex and realistic scenarios.

CRediT authorship contribution statement

Valeria Figueroa: Writing – original draft, Validation, Investigation, Formal analysis, Data curation. **Brenda Velasco:** Validation, Investigation, Formal analysis. **Lilia G. Arellano:** Validation, Investigation, Formal analysis. **Vicente Domínguez-Arca:** Visualization, Validation, Formal analysis, Data curation. **Adriana Cambón:** Visualization, Validation, Methodology. **Alberto Pardo:** Writing – original draft, Visualization, Validation, Software, Data curation. **Antonio Topete:** Writing – review & editing, Validation, Methodology, Formal analysis, Conceptualization. **Luis C. Rosales-Rivera:** Writing – review & editing, Methodology, Conceptualization. **J.F. Armando Soltero:** Writing – review & editing, Resources, Conceptualization. **Silvia Barbosa:** Writing – review & editing, Writing – original draft, Resources, Conceptualization. **Pablo Taboada:** Writing – review & editing, Software, Resources, Conceptualization.

Declaration of competing interest

The authors declare that they have no known competing financial interests or personal relationships that could have appeared to influence the work reported in this paper.

Data availability

Data will be made available on request.

Acknowledgements

Authors thank Agencia Estatal de Investigación (AEI) by project PID2019-109517RB-I00 and Xunta de Galicia for financial support through action ED431C 2022/18. European Regional Development Fund (ERDF) are also acknowledged.

References

[1] C. Fornaguera, M.J. García-Celma, Personalized nanomedicine: a revolution at the nanoscale, J. Pers. Med. 7 (2017) 12, https://doi.org/10.3390/jpm7040012.
[2] R. Van der Meel, E. Sulheim, Y. Shi, F. Kiessling, W.J.M. Mulder, T. Lammers, Smart cancer nanomedicine, Nat. Nanotechnol. 14 (2019) 1007–1017, https://doi.org/10.1038/s41565-019-0567-y.
[3] J. Wu, The enhanced permeability and retention (EPR) effect: the significance of the concept and methods to enhance its application, J. Pers. Med. 11 (2021) 771, https://doi.org/10.3390/jpm11080771.
[4] M.J. Akhtar, M. Ahamed, H.A. Alhadlaq, S.A. Alrokayan, S. Kumar, Targeted anticancer therapy: overexpressed receptors and nanotechnology, Clin. Chim. Acta 436 (2014) 78–92, https://doi.org/10.1016/j.cca.2014.05.004.
[5] K. Prapainop, D.P. Witter, P. Wentworth, A chemical approach for cell-specific targeting of nanomaterials: small-molecule-initiated misfolding of nanoparticle corona proteins, J. Am. Chem. Soc. 134 (2012) 4100–4103, https://doi.org/10.1021/ja300537u.
[6] L. Arellano-Galindo, E. Villar-Alvarez, A. Varela, V. Figueroa, J. Fernandez-Vega, A. Camón, G. Prieto, S. Barbosa, P. Taboada, Hybrid gold nanorod-based nanoplatform with chemo and photothermal activities for bimodal cancer therapy, Int. J. Mol. Sci. 23 (2021) 13109, https://doi.org/10.3390/ijms232113109.
[7] S.-Y. Lee, M.-J. Shieh, Platinum(II) drug-loaded gold nanoshells for chemo-photothermal therapy in colorectal cancer, ACS Appl. Mater. Interfaces 12 (2020) 4254–4264, https://doi.org/10.1021/acsami.9b18855.
[8] B. Pelaz, P. del Pino, P. Maffre, R. Hatmann, M. Gallego, S. Rivera-Fernández, J. M. de la Fuente, G.U. Nienhaus, W.J. Parak, Surface functionalization of nanoparticles with polyethylene glycol: effects on protein adsorption and cellular uptake, ACS Nano 9 (2015) 6996–7008, https://doi.org/10.1021/acsnano.5b01326.
[9] X. Huang, I.H. El-Sayed, W. Qian, M.A. El-Sayed, Cancer cell imaging and photothermal therapy in the near-infrared region by using gold nanorods, J. Am. Chem. Soc. 128 (2006) 2115–2120, https://doi.org/10.1021/ja057254a.
[10] J. Zheng, X. Cheng, H. Zhang, X. Bai, R. Ai, L. Shao, J. Wang, Gold nanorods: the most versatile plasmonic nanoparticles, Chem. Rev. 121 (2021) 13342–13453, https://doi.org/10.1021/acs.chemrev.1c00422.
[11] A.C. Anselmo, S. Mitragotri, A review of clinical translation of inorganic nanoparticles, AAPS J. 17 (2015) 1041–1054, https://doi.org/10.1208/s12248-015-9780-2.

[12] E. Hemmer, A. Benayas, F. Légaré, F. Vetrone, Exploiting the biological windows: current perspectives on fluorescent bioprobes emitting above 1000 nm, Nanoscale Horiz. 1 (2016) 168–184, https://doi.org/10.1039/C5NH00073D.

[13] S. Wan, P.M. Kelly, E. Mahon, H. Stöckmann, P.M. Rudd, F. Caruso, K.A. Dawson, Y. Yan, M.P. Monopoli, The 'sweet' side of the protein corona: effects of glycosylation on nanoparticle-cell interactions, ACS Nano 9 (2015) 2157–2166, https://doi.org/10.1021/nn506060q.

[14] D.F. Moyano, K. Saha, G. Prakash, B. Yan, H. Kong, M. Yazdani, V.M. Rotello, Fabrication of corona-free nanoparticles with tunable hydrophobicity, ACS Nano 8 (2014) 6748–6755, https://doi.org/10.1021/nn5006478.

[15] E. Polo, M. Collado, B. Pelaz, P. del Pino, Advances toward more efficient targeted delivery of nanoparticles *in Vivo*: understanding interactions between nanoparticles and cells, ACS Nano 11 (2017) 2397–2402, https://doi.org/10.1021/acsnano.7b01197.

[16] I. Lynch, A. Salvati, K.A. Dawson, Protein-nanoparticle interactions: what does the cell see? Nat. Nanotechnol. 4 (2009) 546–547, https://doi.org/10.1038/nnano.2009.248.

[17] S. Li, Z. Peng, R.M. Leblanc, Method to determine protein concentration in the protein-nanoparticle conjugates aqueous solution using circular dichroism spectroscopy, Anal. Chem. 87 (2015) 6455–6459, https://doi.org/10.1021/acs.analchem.5b01451.

[18] S. Goy-López, J. Juárez, M. Alatorre-Meda, E. Casals, V.F. Puntes, P. Taboada, V. Mosquera, Physicochemical characteristics of protein–np bioconjugates: the role of particle curvature and solution conditions on human serum albumin conformation and fibrillogenesis inhibition, Langmuir 28 (2012) 9113–9126, https://doi.org/10.1021/la300402w.

[19] J. Piella, N.G. Bastús, V. Puntes, Size-dependent protein-nanoparticle interactions in citrate-stabilized gold nanoparticles: the emergence of the protein corona, Bioconj. Chem. 18 (2017) 88–97, https://doi.org/10.1021/acs.bioconjchem.6b00575.

[20] R. García-Alvarez, M. Hadjidemetriou, A. Sánchez-Iglesias, L. Liz-Marzán, K. Kosterelos, *In vivo* formation of protein corona on gold nanoparticles. The effect of size and shape, *Nanoscale* 10 (2018) 1256–1264, https://doi.org/10.1039/C7NR08322J.

[21] A. Tukova, Y. Nie, Y. Tavakkoli, M. Yaraki, N.T. Tran, J. Wang, A. Rodger, Y. Gu, Y. Wang, Shape dependent protein-induced stabilization of gold nanoparticles: from a protein corona perspective, Aggregate (2023) e323.

[22] C.D. Walkey, J.B. Olsen, H. Guo, A. Emili, W.C.W. Chan, Nanoparticle size and surface chemistry determine serum protein adsorption and macrophage uptake, J. Am. Chem. Soc. 134 (2012) 2139–2147, https://doi.org/10.1021/ja2084338.

[23] C.C. Fleischer, C.K. Payne, Nanoparticle surface charge mediates the cellular receptors used by protein-nanoparticle complexes, J. Phys. Chem. B 116 (2012) 8901–8907, https://doi.org/10.1021/jp304630q.

[24] L.E. González-García, M.N. MacGregor, R.M. Visalakshan, A. Lazarian, A. A. Cavallaro, S. Morsbach, A. Miercynska-Vasiliev, V. Mailänder, K. Landfester, K. Vasilev, Nanoparticles surface chemistry influence on protein corona composition and inflammatory responses, Nanomaterials 12 (2022) 682, https://doi.org/10.3390/nano12040682.

[25] M. Xu, M.G. Soliman, X. Sun, B. Pelaz, N. Feliu, W.J. Parak, S. Liu, How entanglement of different physicochemical properties complicates the prediction of *in Vitro* and *in Vivo* interactions of gold nanoparticles, ACS Nano 12 (2018) 10104–10113, https://doi.org/10.1021/acsnano.8b04906.

[26] K. Saha, M. Rahimi, M. Yazdani, S.T. Kim, D.F. Moyano, S. Hou, R. Das, R. Mout, F. Rezaee, M. Mahmoudi, V.M. Rotello, Regulation of macrophage recognition through the interplay of nanoparticle surface functionality and protein corona, ACS Nano 10 (2016) 4421–4430, https://doi.org/10.1021/acsnano.6b00053.

[27] S. Schöttler, G. Becker, S. Winzen, T. Steinbach, K. Mohr, K. Landfester, V. Mailänder, F.R. Wurm, Protein adsorption is required for stealth effect of poly (ethylene glycol)- and poly(phosphoester)-coated nanocarriers, Nat. Nanotechnol. 11 (2016) 372–377, https://doi.org/10.1038/nnano.2015.330.

[28] S. Hirn, M. Semmler-Behnke, C. Schleh, A. Wenk, J. Lipka, M. Schäffler, S. Takenaka, W. Möller, G. Schmid, U. Simon, W.G. Kreyling, Particle size-dependent and surface charge-dependent biodistribution of gold nanoparticles after intravenous administration, Eur. J. Pharm. Biopharm. 77 (2011) 407–416, https://doi.org/10.1016/j.ejpb.2010.12.029.

[29] Z.J. Deng, M. Liang, I. Toth, M. Monteiro, R.F. Minchin, Plasma protein binding of positively and negatively charged polymer-coated gold nanoparticles elicits different biological responses, Nanotoxicology 7 (2013) 314–322, https://doi.org/10.3109/17435390.2012.655342.

[30] A. Nandakumar, W. Wei, G. Siddiqui, H. Tang, Y. Li, A. Kakinen, X. Wan, K. Koppel, S. Lin, T.P. Davis, D.T. Leong, D.J. Creek, F. Ding, Y. Song, P.C. Ke, Dynamic protein corona of gold nanoparticles with an evolving morphology, ACS Appl. Mater. Interfaces 13 (2021) 58238–58251, https://doi.org/10.1021/acsami.1c19824.

[31] N.D. Burrows, S. Harvey, F.A. Idesis, C.J. Murphy, Understanding the seed-mediated growth of gold nanorods through a fractional factorial design of experiments, Langmuir 33 (2017) 1891–1907, https://doi.org/10.1021/acs.langmuir.6b03606.

[32] J. Hühn, C. Carrillo-Carrión, M.G. Soliman, C. Pfeiffer, D. Valdeperez, A. Masood, I. Chakraborty, L. Zhu, M. Gallego, Z. Yue, M. Carril, N. Feliu, A. Escudero, A. M. Alkilany, B. Pelaz, P. del Pino, W.J. Parak, Selected standard protocols for the synthesis, phase transfer, and characterization of inorganic colloidal nanoparticles, Chem. Mater. 29 (2017) 399–461, https://doi.org/10.1021/acs.chemmater.6b04738.

[33] C.N. Pace, F. Vajdos, L. Fee, G. Grimsley, T. Gray, How to measure and predict the molar absorption coefficient of a protein, Protein Sci. 4 (1995) 2411–2423, https://doi.org/10.1002/pro.5560041120.

[34] H. Liu, N. Pierre-Pierre, Q. Huo, Dynamic light scattering for gold nanorod size characterization and study of nanorod-protein interactions, Gold Bull. 45 (2009) 187–195, https://doi.org/10.1007/s13404-012-0067-4.

[35] S. Tunç, O. Duman, The effect of different molecular weight of poly(ethylene glycol) on the electrokinetic and rheological properties of na-bentonite suspensions, Colloids Surf. a: Physicochem. Eng. Aspects 317 (2008) 93–99, https://doi.org/10.1016/j.colsurfa.2007.09.039.

[36] T. Kitano, S. Kawaguchi, K. Ito, A. Minakata, Dissociation behavior of poly(fumaric acid) and poly(maleic acid). 1. potentiometric titration and intrinsic viscosity, Macromolecules 20 (1987) 1598–1606, https://doi.org/10.1021/ma00173a028.

[37] C. Yu, L. Varghese, J. Irudayaraj, Surface modification of cetyltrimethylammonium bromide-capped gold nanorods to make molecular probes, Langmuir 23 (2007) 9114–9119, https://doi.org/10.1021/la701111e.

[38] E. Casals, T. Pfaller, A. Duschl, G.J. Oostingh, V. Puntes, Time evolution of the nanoparticle protein corona, ACS Nano 4 (2010) 3623–3632, https://doi.org/10.1021/nn901372t.

[39] R.A. Sperling, T. Liedl, S. Duhr, S. Kudera, M. Zanella, C.-A. Lin, W.H. Chang, D. Braun, W.J. Parak, Size determination of (bio)conjugated water-soluble colloidal nanoparticles: a comparison of different techniques, J. Phys. Chem. C 111 (2007) 11552–11559, https://doi.org/10.1021/jp070999d.

[40] H. Lee, A.H. de Vries, S.-J. Marrink, R.W. Pastor, A coarse-grained model for polyethylene oxide and polyethylene glycol: conformation and hydrodynamics, J. Phys. Chem. B 113 (2009) 13186–13194, https://doi.org/10.1021/jp9058966.

[41] K. Partikel, R. Korte, N.C. Stein, D. Mulac, F.C. Herrmann, H.-U. Humpf, K. Langer, Effect of nanoparticle size and PEGylation on the protein corona of PLGA nanoparticles, Eur. J. Pharm. Biopharm. 141 (2019) 70–80, https://doi.org/10.1016/j.ejpb.2019.05.006.

[42] D. Selli, S. Motta, C. Di Valentin, Impact of surface curvature, grafting density and solvent type on the PEGylation of titanium dioxide nanoparticles, J. Colloid Interface Sci. 555 (2019) 519–531, https://doi.org/10.1016/j.jcis.2019.07.106.

[43] C. Kinnear, H. Dietsch, M.J.D. Clift, C. Endes, B. Rothen-Rutishauser, A. Petri-Fink, Gold nanorods: controlling their surface chemistry and complete detoxification by a two-step place exchange, Angew. Chem. Int. Ed. 52 (2013) 1934–1938, https://doi.org/10.1002/anie.201208568.

[44] B.D. Fairbanks, M.P. Schwartz, C.N. Bowman, K.S. Anseth, Photoinitiated polymerization of PEG-diacrylate with lithium phenyl-2,4,6-trimethylbenzoylphosphinate: polymerization rate and cytocompatibility, Biomaterials 30 (2009) 6702–6707, https://doi.org/10.1016/j.biomaterials.2009.08.055.

[45] V. Mirshafiee, R. Kim, S. Park, M. Mahmoudi, M.L. Kraft, Impact of protein pre-coating on the protein corona composition and nanoparticle cellular uptake, Biomaterials 75 (2016) 295–304, https://doi.org/10.1016/j.biomaterials.2015.10.019.

[46] V.H. Nguyen, B.-J. Lee, Protein corona: a new approach for nanomedicine design, Int. J. Nanomed. 12 (2017) 3137–3151, https://doi.org/10.2147/IJN.S129300.

[47] J.W. Weisel, R.I. Litvinov, Fibrin formation, structure and properties, Subcel Biochem. 82 (2017) 405–456, https://doi.org/10.1007/978-3-319-49674-0_13.

[48] T. Cedervall, I. Lynch, S. Lindman, S. Linse, Understanding the nanoparticle–protein corona using methods to quantify exchange rates and affinities of proteins for nanoparticles, Proc. Natl. Acad. Sci. 104 (2007) 2050–2055, https://doi.org/10.1073/pnas.0608582104.

[49] X. Zhao, R. Liu, Y. Teng, X. Liu, The Interaction between Ag+ and bovine serum albumin: a spectroscopic investigation, Sci. Total Environ. 409 (2011) 892–897, https://doi.org/10.1016/j.scitotenv.2010.11.004.

[50] L. Shang, Y. Wang, J. Jiang, S. Dong, pH-dependent protein conformational changes in albumin: gold nanoparticle bioconjugates: a spectroscopic study, Langmuir 23 (2007) 2714–2721, https://doi.org/10.1021/la062064e.

[51] G. Yohannes, S.K. Wiedmer, M. Elomaa, M. Jussila, V. Aseyev, M.-L. Riekkola, Thermal aggregation of bovine serum albumin studied by asymmetrical flow field-flow fractionation, Anal. Chim. Acta 675 (2010) 191–198, https://doi.org/10.1016/j.aca.2010.07.016.

[52] Z. Adamczyk, J. Barbasz, M. Ciesl, Mechanisms of fibrinogen adsorption at solid substrates, Langmuir 27 (2011) 6868–6878, https://doi.org/10.1021/la200798d.

[53] N. Orellana, S. Palma, E. Torres, M.L. Cordero, V. Vio, J.M. Ruso, J. Juárez, A. Topete, E. Araya, R. Vasquez-Contreras, M.J. Kogan, N. Hassan, Study of the interaction of folic acid-modified gold nanorods and fibrinogen through microfluidics: implications for protein adsorption, incorporation and viability of cancer cells, Nanoscale 13 (2021) 17807–17821, https://doi.org/10.1039/D1NR03179A.

[54] A.M. Merlot, D.S. Kalinowski, D.R. Richardson, Unraveling the mysteries of serum albumin—more than just a serum protein, Front. Physiol. 5 (2014) 299, https://doi.org/10.3389/fphys.2014.00299.

[55] B.H. Shaz, C.D. Hillyer, Chap. 123, in: Transfusion Medicine and Hemostasis, second ed., Elsevier, The Netherlands, 2013, pp. 793–798.

[56] J. Deng, M. Sun, J. Zhu, C. Gao, Molecular interactions of different size AuNP–COOH nanoparticles with human fibrinogen, Nanoscale 5 (2013) 8130–8137, https://doi.org/10.1039/c3nr02327c.

[57] S.H. De Paoli-Lacerda, J.J. Park, C. Meuse, D. Pristinski, M.L. Becker, A. Karim, J. F. Douglas, Interaction of gold nanoparticles with common human blood proteins, ACS Nano 4 (2010) 365–379, https://doi.org/10.1021/nn9011187.

[58] M. De, C.-C. You, S. Srivastava, V.M. Rotello, Biomimetic interactions of proteins with functionalized nanoparticles: a thermodynamic study, J. Am. Chem. Soc. 129 (2007) 10747–10753, https://doi.org/10.1021/ja071642q.

[59] D. Hühn, K. Kantner, C. Geidel, S. Brandholt, I. De Cock, S.J.H. Soenen, P. Rivera-Gil, J.-M. Montenegro, K. Braeckmans, K. Müllen, G.U. Nienhaus, M. Klapper, W. J. Parak, Polymer-coated nanoparticles interacting with proteins and cells: focusing on the sign of the net charge, ACS Nano 7 (2013) 3253–3263, https://doi.org/10.1021/nn3059295.

[60] E. Polo, V. Araban, B. Pelaz, A. Alvarez, P. Taboada, M. Mahmoudi, P. del Pino, Photothermal effects on protein adsorption dynamics of PEGylated gold nanorods, Appl. Mater. Today 15 (2019) 599–604, https://doi.org/10.1016/j.apmt.2019.04.013.

[61] N. Shimokhina, A. Bronowska, S.W. Homan, Contribution of ligand desolvation to binding thermodynamics in a ligand-protein interaction, Angew. Chem. Int. Ed. 45 (2006) 6374–6376, https://doi.org/10.1002/anie.200602227.

[62] U.C. Anozie, K.J. Quigley, A. Prescott, S.M. Abel, P. Dalhaimer, Equilibrium binding of isolated and in-plasma high-density lipoproteins (HDLs) to polystyrene nanoparticles, J. Nanoparticle Res. 22 (2020) 223, https://doi.org/10.1007/s11051-020-04953-0.

[63] Z. Wang, Q. Zhao, M. Cui, S. Pang, J. Wang, Y. Liu, L. Xie, Probing temperature- and pH-dependent binding between quantum dots and bovine serum albumin by fluorescence correlation spectroscopy, Nanomaterials 7 (2017) 93, https://doi.org/10.3390/nano7050093.

[64] A.L. Lira, N. Mina, C.R. Bonturi, R.S. Nogueira, R.J.S. Torquato, M.L.V. Oliva, A. A. Sousa, Anionic ultrasmall gold nanoparticles bind to coagulation factors and disturb normal hemostatic balance, Chem. Res. Toxicol. 35 (2022) 1558–1569, https://doi.org/10.1021/acs.chemrestox.2c00190.

[65] M. Waghmare, B. Khade, P. Chaudhari, P. Dongre, Multiple layer formation of bovine serum albumin on silver nanoparticles revealed by dynamic light scattering and spectroscopic techniques, J. Nanoparticle Res. 20 (2018) 185, https://doi.org/10.1007/s11051-018-4286-3.

[66] P. Roach, D. Farrar, C.C. Perry, Surface tailoring for controlled protein adsorption: effect of topography at the nanometer scale and chemistry, J. Am. Chem. Soc. 128 (2006) 3939–3945, https://doi.org/10.1021/ja056278e.

[67] G.M. Mortimer, N.J. Butcher, A.W. Musumeci, Z.J. Deng, D.J. Martin, R. F. Minchin, Cryptic epitopes of albumin determine mononuclear phagocyte system clearance of nanomaterials, ACS Nano 8 (2014) 3357–3366, https://doi.org/10.1021/nn405830g.

[68] I. Ottonelli, J.T. Duskey, F. Genovese, F. Pederzoli, R. Caraffi, M. Valenza, G. Tosi, M.A. Vandelli, B. Ruozi, Quantitative comparison of the protein corona of nanoparticles with different matrices, Int. J. Pharm. X 4 (2022) 100136, https://doi.org/10.1016/j.ijpx.2022.100136.

[69] M.M. Lopez, D. Kosk-Kosicka, Spectroscopic analysis of halothane binding to the plasma membrane Ca2+-ATPase, Biophys. J. 74 (1998) 974–980, https://doi.org/10.1016/S0006-3495(98)74020-74022.

[70] W. Ruankham, K. Phopin, R. Pingaew, S. Prachayasittikul, V. Prachayasittikul, T. Tantimongcolwat, In Silico and multi-spectroscopic analyses on the interaction of 5-amino-8-hydroxyquinoline and bovine serum albumin as a potential anticancer agent, Sci. Rep. 11 (2021) 20187, https://doi.org/10.1038/s41598-021-99690-2.

[71] M.G. Sandros, D. Gao, C. Gokdemir, D.E. Benson, General, high-affinity approach for the synthesis of fluorophore appended protein nanoparticle assemblies, Chem. Commun. 22 (2005) 2832–2834, https://doi.org/10.1039/B501315A.

[72] L.C.P. Gonçalves, Photophysical properties and therapeutic use of natural photosensitizers, J. Photochem. Photobiol. 7 (2021) 100052, https://doi.org/10.1016/j.jpap.2021.100052.

[73] I. Parastatidis, L. Thomson, A. Burke, I. Chernysh, C. Nagaswami, J. Visser, S. Stamer, D.C. Liebler, G. Koliakos, H.F.G. Heijnen, G.A. Fitzgerald, J.W. Weisel, H. Ischiropoulos, Fibrinogen β-chain tyrosine nitration is a prothrombotic risk factor, J. Biol. Chem. 283 (2008) 33848–33853, https://doi.org/10.1074/jbc.M805522200.

[74] J.R. Lakowicz, Principles of Fluorescence Spectroscopy, Springer, US, Boston, MA, 2006.

[75] X. Zhang, J. Zhang, F. Zhang, S. Yu, Probing the binding affinity of plasma proteins adsorbed on Au nanoparticles, Nanoscale 9 (2017) 4787–4792, https://doi.org/10.1039/C7NR01523B.

[76] G. Wang, C. Yan, S. Gao, Y. Liu, Surface chemistry of gold nanoparticles determines interactions with bovine serum albumin, Mater. Sci. Eng. C 103 (2019) 109856, https://doi.org/10.1016/j.msec.2019.109856.

[77] J. Beurton, P. Lavalle, A. Pallotta, T. Chaigneau, I. Clarot, A. Boudier, Design of surface ligands for blood compatible gold nanoparticles: effect of charge and binding energy, Int. J. Pharm. 580 (2020) 119244, https://doi.org/10.1016/j.ijpharm.2020.119244.

[78] W. Shang, J.H. Nuffer, V.A. Muñiz-Papandrea, W. Colón, R.W. Siegel, J.S. Dordick, Cytochrome c on silica nanoparticles: influence of nanoparticle size on protein structure, stability, and activity, Small 5 (2009) 470–476, https://doi.org/10.1002/smll.200800995.

[79] Z.J. Deng, M. Liang, I. Toth, M.J. Monteiro, R.F. Minchin, Molecular interaction of poly(acrylic acid) gold nanoparticles with human fibrinogen, ACS Nano 6 (2012) 8962–8969, https://doi.org/10.1021/nn3029953.

[80] G. Wang, W. Wang, E. Shangguan, S. Gao, Y. Liu, Effects of gold nanoparticle morphologies on interactions with proteins, Mater. Sci. Eng. C 111 (2020) 110830, https://doi.org/10.1016/j.msec.2020.110830.

[81] W.K. Surewicz, H.H. Mantsch, D. Chapman, Determination of protein secondary structure by Fourier transform infrared spectroscopy: a critical assessment, Biochemistry 32 (1993) 389–394, https://doi.org/10.1021/bi00053a001.

[82] J. Juárez, P. Taboada, S. Goy-López, A. Cambón, M.-B. Madec, S.G. Yeates, V. Mosquera, Additional supra-self-assembly of human serum albumin under amyloid-like-forming solution conditions, J. Phys. Chem. B 113 (2009) 12391–12399, https://doi.org/10.1021/jp904167e.

[83] J. Juárez, M. Alatorre-Meda, A. Cambón, A. Topete, S. Barbosa, P. Taboada, V. Mosquera, Hydration effects on the fibrillation process of a globular protein: the case of human serum albumin, Soft Matter 8 (2012) 3608–3619, https://doi.org/10.1039/C2SM06762E.

[84] M.J. Hajipour, J. Raheb, O. Akhavan, S. Arjmand, O. Mashinchian, M. Rahman, M. Abdolahad, V. Serpooshan, S. Laurent, M. Mahmoudi, Personalized disease-specific protein corona influences the therapeutic impact of graphene oxide, Nanoscale 7 (2015) 8978–8994, https://doi.org/10.1039/C5NR00520E.

[85] P. Roach, D. Farrar, C.C. Perry, Interpretation of protein adsorption: surface-induced conformational changes, J. Am. Chem. Soc. 127 (2005) 8168–8173, https://doi.org/10.1021/ja042898o.